Spring 5-2011

The Measurement of Bone Quality in Medical Images Using Statistical Textural Features

Ning Huang

THE MEASUREMENT OF BONE QUALITY IN MEDICAL IMAGES USING STATISTICAL TEXTURAL FEATURES

by

NING HUANG

A thesis submitted in partial fulfillment
of the requirements for the degree of
Masters of Science in Electrical Engineering
Department of Electrical Engineering

Mukul Shirvaikar, Ph. D. Committee Chair

College of Engineering and Computer Science

The University of Texas at Tyler
May 2011

The University of Texas at Tyler
Tyler, Texas

This is to certify that the Master's thesis of

NING HUANG

has been approved for the thesis requirements on
May 12, 2011
for the Masters of Science in Electrical Engineering degree

Approvals:

Thesis Chair: Mukul V. Shirvaikar, Ph. D.

Member: Xuanliang Dong, Ph. D.

Member: Ron J. Pieper, Ph. D.

Chair and Graduate Coordinator: Mukul V. Shirvaikar, Ph. D.

Dr. James K. Nelson, Jr.
Dean, College of Engineering and Computer Science

Acknowledgements

First and foremost, I thank my Aunt Nancy Lin and Uncle Morris Smith for their constant coaching to me through life and their financial support. I am grateful to Dr. Mukul Shirvaikar and Xuanliang Dong who gave me the chance to work on this project. I also express my gratitude to them for their time and patience for assisting me through this thesis. I am appreciative to Dr. Ron Pieper for taking time to be a part of my committee and reviewing my work.

Table of Contents

List of Figures

List of Tables

Abstract

THE MEASUREMENT OF BONE QUALITY IN MEDICAL IMAGES USING STATISTICAL TEXTURAL FEATURES

Ning Huang

Thesis Chair: Mukul Shirvaikar, Ph. D.

The University of Texas at Tyler
May 2011

Mineral density and bone architecture properties are the main measures of bone quality. Dual-energy X-ray Absorptiometry (DXA) is the traditional clinical measurement technique for bone mineral density, but it is insensitive to architectural information. Image analysis of the architectural properties of bones can be used to predict bone quality. This study is aimed at investigating the statistical parameters extracted from two-dimensional projection images of the DXA scans and exploring its link with architectural properties, and its correlation with a bone's mechanical properties.

In this research, features extracted from the Gray Level Co-occurrence Matrix (GLCM) for a 2D image are compared with features extracted from semivariogram analysis in order to estimate bone micro-architectural and mechanical properties. Data analysis was conducted on 13 trabecular bones of different strengths (with an in-plane

spatial resolution of about 50μm). Ground truth data for bone volume fraction (BV/TV), bone strength and elasticity was available for the dataset, based on complex 3D analysis and mechanical tests.

Correlation between the statistical parameters and biomechanical test results was studied using regression analysis. The results showed that the cluster-shade parameter extracted from the GLCM was strongly correlated with the microstructure of the trabecular bone and also somewhat related to the mechanical properties. Additionally, a parameter called 'sill' obtained by the semivariogram method was found to be highly associated with the mechanical properties of the bone and slightly related to its micro-architectural properties.

Chapter One

Introduction

Dual-energy X-ray Absorptiometry (DEXA) is one of the most popular ways of estimating bone strength and fracture risk in bone loss diseases such as osteoporosis. This is because it can test bone mass loss which would be the result of osteoporotic changes. But the DEXA's insensitivity to architectural changes masks an important factor contributing to bone strength which cannot be ignored. The new methods of 3D image analysis such as stereology principles, which provide architectural information are so costly that they are impractical as a solution. Researchers are developing new practical techniques which are based on mathematical analysis of the two dimensional plain-projection image obtained from the three-dimensional tissue images of the DEXA.

Texture information could be extracted by statistical analysis of these two dimensional images. 'Texture' as it is used in this context refers to the visual effect produced by the spatial distribution of pixel value variation over relatively small areas [1]. Textural information can be either coarse or smooth. The coarseness index is related to the spatial repetition period of the local structure. Textural information translated into the bone’s microstructure can be seen in the bone's volume fraction. It can also be perceived in other properties of the image.

Texture has been proven to be a function of second-order statistics. The computation of gray level co-occurrence matrix (GLCM) as a second-order texture measure is one of the popular methods in texture analysis. Several statistical parameters can be extracted from the GLCM, to quantify the spatial relationship between pixels within the area under investigation. In order to qualify characteristics of a bone, different

GLCM features including energy, contrast, entropy, autocorrelation, correlation, inverse difference moment, cluster shade are studied [1, 2]. The intent is to identify a measure of bone strength so that fracture risk can be assessed numerically.

The semivariogram is another method that can be applied to two dimensional plain-projection images and is based on Markov random fields (MRF). It is used to indicate spatial correlation in observations of measured pairs of sampled locations. Exponential models were built on the semivariogram function to analyze the biomechanical character of the bone.

Objective and framework

This thesis investigates the relationship between 2D projection images and real bone properties. GLCM and semivariogram algorithms were designed in MATLAB and the methods are compared. The comparison criteria is the coefficient of determination R^2 based on linear regression models.

Organization of the thesis

This thesis is divided into six chapters. Chapter 2 discusses technical background including texture definition and introduction of two application algorithms. Chapter 3 gives the sequence of image analysis. Chapter 4 describes the details of materials and of experiments of GLCM and semivariogram. Chapter 5 lists and analyzes the results of the experiments. Chapter 6 includes discussion and conclusion.

Chapter Two

Technical Background

Trabecular structure is important in osteoporosis clinical applications. Turner [3] has proved that incorporating both density and architecture can improve the bone strength predictability to 90%. Two-dimensional projection of the bone images can be utilized to measure “texture”. Luoand Kinney [4] show that texture information related to trabecular structure is conserved during the transformation from 3D to 2D images using software analysis. Many texture analysis algorithms have been applied to bone images to estimate their architecture quantitatively. Fractal analysis of X-ray textures has been used for identification of osteoporotic patients [5, 6]. Chappard [7] uses run-length distribution texture analysis methods on X-ray radiographs to prove that it is a reliable descriptor of bone loss in a rat bone model.

GLCM has become an increasingly popular texture analysis method since the original study by Haralick [1]. Many researchers have applied it to the geosciences and remote sensing fields such as SAR sea ice [8, 9], desert [10], cloud [11, 12] and so on. It is a relatively new method for texture analysis in 2D projections of bone images [13]. As a result, this method has a lot of potential for exploration. Another popular method based on MRFs is the semivariogram. This is key function utilized in geostatistics [14, 15] but has been recently applied to 2D projection bone analysis. Dong [16] has used it to fit a model of the spatial correlation of the observed phenomenon in trabecular bones.

The goal in this project is to use GLCM based features to detect its parameters and its relationship with quality of bone and compare it to the semivariogram method.

2.1 Definition of Texture

Texture is the quality of an object which we sense through touch or feel. Textures are of many kinds: smooth and coarse, cold and warm, soft and hard, wet and dry (figure 2.1). In fact, any tactile sensation we can imagine is a texture. In other words, all surfaces can be described in terms of texture.

(a) (b)

Figure 2.1(a) Texture information including sunshine (b) texture information including cold weather

From Figure 2.1(a) a lot of textural information can be derived: sunshine, green trees, cars, yellow clock tower, grass lawn, and so on. Figure 2.1(b) also includes textural information: cold weather, snow, trees, tower covered with snow. It is easier to derive more textural information from Figure 2.1(a) than Figure 2.1(b). A wealth of information can be derived from the image based on spatial relationship features: the distance between two cars, tower height, trees size etc.

In this research, the hypothesis presented is that textural features obtained from images of bones will be a strong indicator of micro-architecture or mechanical properties. This hypothesis is based upon observations of bone images of varying strengths (Appendix B). There are two components contained in the texture information; one is pixel value, the other is its spatial inter dependence of pixel values. The variability of pixel values will demonstrate spatial dependence in most cases. That means the pixel values are correlated in the image based on location and orientation [1, 2]. This spatial dependence is deeply related with the micro-architecture of bone tissue under study. Meanwhile, we can also extract additional texture information such as mechanical properties of bone from the texture algorithms.

There are many statistical texture algorithms intended to characterize and identify textures; for example, GLCM [1, 2], semivariograms [13, 14], gray-level run length [17], gray-level difference vector [18], max-min texture [19], sum and difference histograms [20], texture spectrum [21] and Fourier power spectrum [22] are among the popular approaches in the literature. We have chosen the GLCM and semivariogram as our texture analysis algorithms to investigate features of 2D projection bone image.

2.2 Gray Level Co-occurrence Matrix (GLCM)

The gray level co-occurrence matrix is a primitive measure of texture [23]. It is a quantitative measure of the second order statistics in an image. The concept of Gray Level Co-occurrence Matrix (GLCM) is introduced with one simple example. The GLCM measures the frequency of different combinations of pixel brightness values (gray

levels) occurring in an image [1, 2]. The definition is as follows, suppose we have an image I to be analyzed in which:

$L_x = \{1, 2, ... N_x\}$ is the number of column,

$L_y = \{1, 2, ... N_y\}$ is the number of rows,

$G = \{0, 1, 2, ... N_{g-1}\}$ is the set of N_g quantized gray levels.

A GLCM is a square matrix for which the number of rows is equal to the number of the columns, and also equal to the number of gray levels. Each element in this new matrix is referred to as a "relative frequency" $g(i, j)$ between 2 pixels with gray levels i and j respectively. An additional condition is that the two pixels to be located at the ends of a predefined vector of length *d* and angle θ (polar representation) or length d_1 and d_2 (cartesian representation). One GLCM can be computed for each new vector $t = (d, \theta)$ and can be named G_t with each element $G_t(i, j)$ being the frequency of occurrence of the pixel value pair (*i, j*).

Figure 2.2 shows an example for computing a GLCM from a sample image. Figure 2.2(a) location wise is the original image with pixels values. Figure 2.2(b) is the 4*4 GLCM matrix with combination pixels values. Figure 2.2(c) shows the GLCM matrix. Row 1 column 1 in Figure 2.2(c) shows the number of (0,0) combinations in the image. The same rule applies to all the other elements in both matrices. Figure 2.2(d) shows each of the elements of Figure 2.2(c) as a probability, given that the total number of possible transitions on Figure 2.2(a) is 12. In this format the GLCM is similar to a second order histogram.

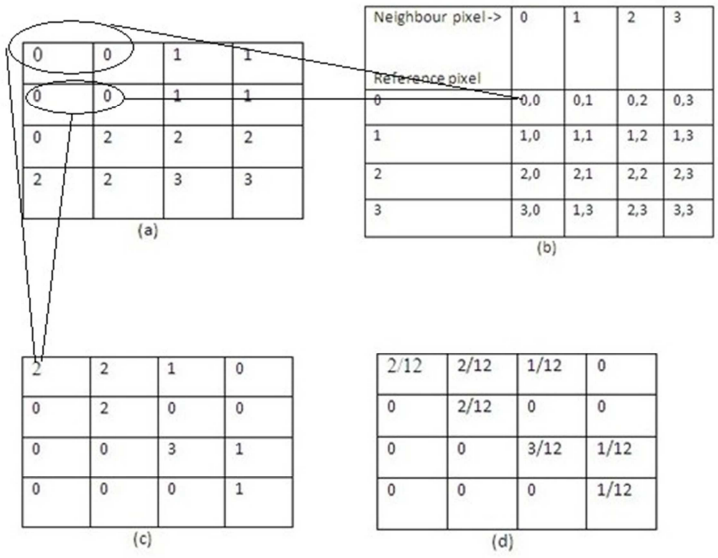

Figure 2.2 GLCM computation example (a) pixel distribution in a sample image (b) location-wise pixel pair (c) GLCM matrix of sample image with d=1, $\theta = 0^0$ (d) GLCM matrix value in the "relative frequency" format

The GLCM matrix represents significant quantity of data as it is typically computed for multiple vector length and directions, consequently, features computed from GLCM matrix are a more attractive option to measure textural information. A number of texture features can be extracted from the GLCM matrix including the first moment μ_x , μ_y and standard deviation "σ"for the GLCM matrix. Let *g (i, j)* be the *(i, j)* directional entry in G, then the means are given by the equation.

$$\mu_x = \sum_{i=0}^{N_g-1} \sum_{j=0}^{N_g-1} i \cdot g(i, j)$$
$$\mu_y = \sum_{i=0}^{N_g-1} \sum_{j=0}^{N_g-1} j \cdot g(i, j) \qquad (2.1)$$

The first moment is not the average of pixel values in the original image [2]. The moments represent the weighted means for the rows and columns of the GLCM. They are identical if the GLCM is symmetrical and will be different if the GLCM is asymmetrical.

$$\sigma_x = \sum_{i=0}^{N_g-1} \sum_{j=0}^{N_g-1} (i-\mu_x)^2 \cdot g(i,j)$$
$$\sigma_y = \sum_{i=0}^{N_g-1} \sum_{j=0}^{N_g-1} (i-\mu_y)^2 \cdot g(i,j) \tag{2.2}$$

The Variance relies on the weighted mean, and the dispersion around the mean within small value. This feature deals specifically with the variance of the probability of pixel pair occurrences and is not the simple variance of gray levels in the original image [2,7].

The seven features that were selected for texture analysis were based on a careful observation of the GLCMs computed from the images in the data set (Appendix C). The features are defined below:

$$A = \sum_{i=0}^{N_g-1} \sum_{j=0}^{N_g-1} g^2(i,j) \tag{2.3}$$

The Energy "*A*" is also called Angular Second Moment [8] and measures the number of repeated pairs. High energy values occur when the gray level distribution in the image is a constant, or when the frequency of repeated pixel pairs is high. Thus, energy reaches values close to its maximum, equal to 1. Energy predicted will be higher for smooth-textures than for rough textures.

$$C = \sum_{i=0}^{N_g-1} \sum_{j=0}^{N_g-1} g(i,j)(i-j)^2 \tag{2.4}$$

The contrast "*C*" is a feature that favors transitions between the highest and the lowest gray level values of pair pixels [24]. This definition is also used in the GLCM

contrast expression also. High contrast values imply high contrast textures. This measure is also known as “Inertia”.

$$E = \sum_{i=0}^{N_g-1} \sum_{j=0}^{N_g-1} g(i,j) \log\{g(i,j)\} \tag{2.5}$$

The Entropy parameter “*E*” measures the disorder within an image. [2]When the image is not texturally uniform, many GLCM elements have very small values, which imply that entropy is very high [2, 8]. Entropy is correlated to energy, thus, similar results are expected for energy and entropy for a given image.

$$H = \sum_{i=0}^{N_g-1} \sum_{j=0}^{N_g-1} g\ (i,j)\left[1/(1+(i-j)^2)\right] \tag{2.6}$$

The inverse difference moment “*H*” is also known as homogeneity [9]. This parameter measures image homogeneity as it assumes larger values for smaller gray level differences in pair elements [2]. Therefore, the parameter is more sensitive to the presence of near diagonal elements in the GLCM.

$$U = \sum_{i=0}^{N_g-1} \sum_{j=0}^{N_g-1} (ij) g(i,j) \tag{2.7}$$

The autocorrelation “*U*” is defined combination pairs as one point or one element, and describes the correlation of this point between other combination pair series.

$$R = \frac{\sum_{i=0}^{N_g-1} \sum_{j=0}^{N_g-1} (ij) g(i,j) - \mu_x - \mu_y}{\sigma_x \sigma_y} \tag{2.8}$$

The GLCM correlation “*R*” is expressed by the correlation coefficient between two random variables *I* and *j*, where *I* represents the possible outcomes in the gray level

value measurement for the first element of the displacement vector, while *j* is associated with the gray level value of the second element of the displacement vector [2].

$$S = \sum_{i=0}^{N_g-1} \sum_{j=0}^{N_g-1} (i + j - \mu_x - \mu_y)^3 \cdot g(i, j) \tag{2.9}$$

The cluster shade "*S*" emphasizes locally shadowed areas, and measures the symmetry of the matrix [25]. It significantly relies on the GLCM sum of row and column moments. It can be positive or negative, determined by with side of the mean was favored. In other words, when the absolute value of cluster shade is high, the GLCM is lacks of symmetry.

2.3 Semivariogram

Statistical prediction may be based on the assumption that a set of measurements of a variable (z_1 , z_2 ,….. z_n) represent *n* realizations of a random variable *z*. The spatial variation can be evaluated using semivariogram [13].The semi-variance (γ) is defined as half of the expected squared difference between any paired data values { $z(x), z(x+h)$ }:

$$\text{var}\left[z(x) - z(x+h)\right] = E\left[\left\{z(x) - z(x+h)\right\}^2\right] = 2\gamma(h) \tag{2.10}$$

In our study, *z* is a random function of the indentation modulus of applied picture that varies continuously in space; *x* is the spatial coordinate of locations; so $z(x)$ is the pixel value of our sample, and *h*, also known as lag, is a vector representing the distance and direction between any two data locations. $h = (d, \theta)$

$$\gamma(h) = \frac{1}{2m(h)} \sum_{i=1}^{m(h)} \left\{z(x_i) - z(x_i + h)\right\}^2 \tag{2.11}$$

m(h) is the number of data pairs { $z(x_i), z(x_i + h)$ } for observations separated by *h*.

For example we have the same image as figure 2.3

0	0	1	1
0	0	1	1
0	2	2	2
2	2	3	3

Figure 2.3 Sample image to compute the semivariogram

If $d=1$, and $\theta=0^{\circ}$, the semivariogram value solution is given below:

$$\gamma(h)\cdot 2m(h)=|0-0|^2+|0-1|^2+|1-1|^2+|0-0|^2+|0-1|^2$$
$$+|1-1|^2+|0-2|^2+|2-2|^2+|2-2|^2+|2-2|^2+|2-3|^2+|3-3|^2=7$$

There are twelve pairs in the image resulting in $m(h)=12$; $\hat{\gamma}(h)=7/24$. According to the geostatistics experience, some model function can be built based on experimental data. These models can be used to describe the common behavior and the general characteristics of a semivariogram[13], including:

- The semivariogram value typically increased with the lag distance
- The semivariogram value will converge to limit constant for the whole picture called “sill” with increasing lag distance
- The value increases rapidly at low lags and then progresses linearly. The lag distance corresponding to changing moment is called the “correlation length”

Many models have been built in the past to fit the features described obtained from the semivariogram. For example: spherical model, exponential model, Gaussian model and so on [13, 14].The exponential models are described by the equation:

$$\gamma(h) = c_0 + c(1 - e^{\frac{-h}{L}}) \quad \gamma(0) = 0 \tag{2.12}$$

where c_0 is the nugget variance, c is "sill", h is the offset between compared pair, γ(h) is the semi-variance as a function of lag (h), and L is the correlation length. The parameters in the exponential model (L, c_0, c) can be estimated by the least square estimation method [13, 14].

Chapter Three

Image Analysis Sequence

Before applying statistical analysis to the bone image, some preprocessing steps are necessary. First, we must convert the 3D image into a 2D projection image. A template image should be created in order to gain the region of interest in the 2D projection image. Considering that one of the purposes is microstructure analysis of the bone images, some methods that can promote image enhancement in the spatial domain should be considered. A common method known as “histogram equalization” is utilized for this purpose. Finally, in order to reduce the calculation time for the algorithms, another commonly used method—“quantization” of gray levels needs to be applied. Figure 3.1 depicts the flow of image preprocessing steps.

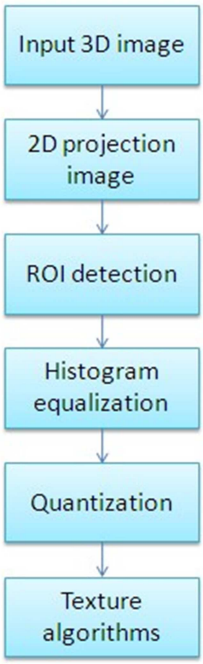

Figure 3.1Image analysis sequence

3.1 Transforming 2D Projection Image

Two-dimensional projection images of bone images can be generated by averaging the gray values of the slice images from the three-dimensional micro-CT data [26]. See figure 3.2.

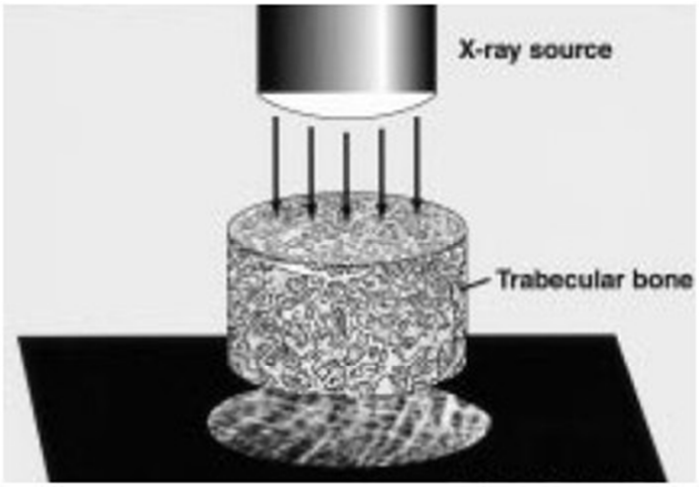

Figure 3.2 Transformation of 3D image into a 2D projection image [26]

3.2 Region of Interest

It is sometimes of interest to process a single subregion of an image, leaving other regions unchanged. This is commonly referred to as region-of-interest (ROI) processing. There are many methods to detect the region of interest. Thresholding is one of the popular methods for this purpose [27]. From a grayscale image, a threshold can be used to create a binary image. The binary image can act as a template for the ROI.

During the threshold process, it is assumed that the ROI pixel value is greater or lower than some threshold value. Normally, an object pixel is given a value of “1” while a background pixel is given a value of “0.” Finally, a template binary image is created by coloring each pixel white or black.

After getting the template binary images from the thresholding process, there may be some spurious areas still existing inside the interest region. The reason for the presence of these spots is that some pixel values in the interest region are below the threshold pixel value. In order to delete these blobs, many morphological methods can be applied, such as “dilation and erosion” [28], “the hit-or-miss transformation” [29], “opening and closing” [29]. A MATLAB function described as “*imfill (p, ‘holes’)*” is utilized in this research. This function fills holes in the binary image *p*. A hole is a set of background pixels that cannot be reached by filling in the background from the edge of the image.

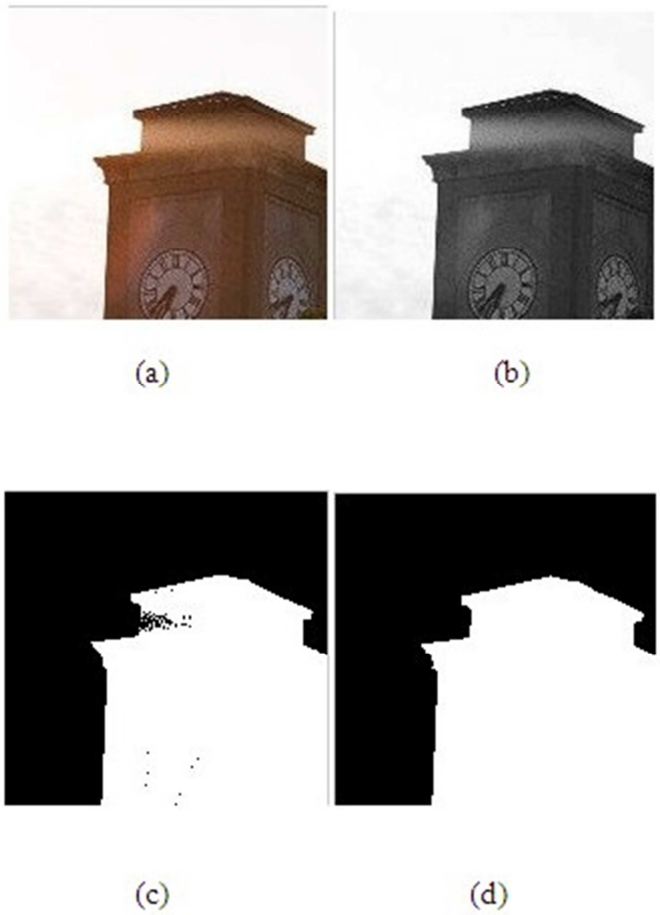

Figure 3.3 (a) Original sample color picture (b) gray scale image of color sample (c) template binary image with “0” inside interest region (d) binary template image after filling process

Figure 3.3(a) is a sample color image composed of tower with sky background. The texture study is to be done on the tower part only. First the color image is transformed to gray scale and then a template image with threshold method, which includes many dark pixels inside the ROI. The template image with “1” in the tower part and “0” in the background is created from the original image. Size and index location is the same as the original image and can be used as a check for the ROI. Figure 3.4 shows the ROI method applied on 2D projection bone image.

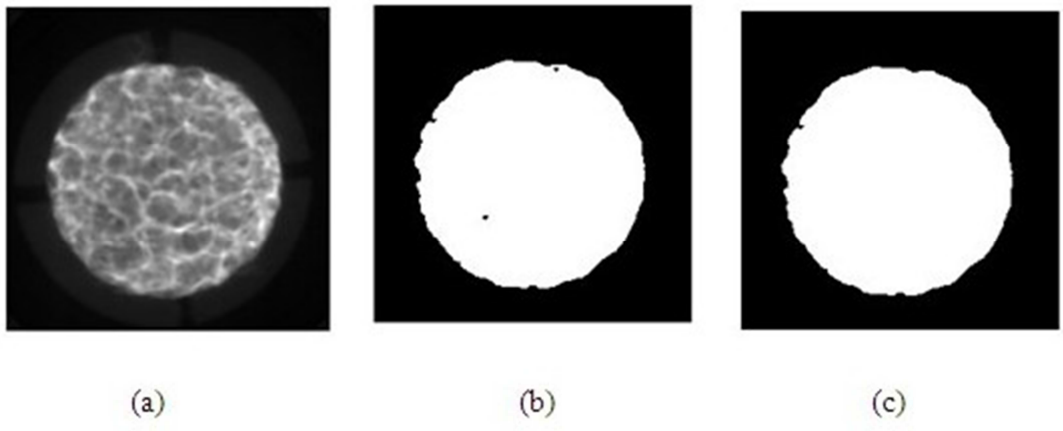

Figure 3.4 (a) Gray scale image of 2D projection bone (b) template binary image with “0” inside interest region (c) binary template image after filling process, white stands for valid bone region

3.3 Histogram Equalization

In image processing, histogram equalization is a popular technique to improve contrast. It has been proved that this method will provide better details of bone structure in X-ray images [26]. Histogram Equalization uses the image's histogram to adjust its contrast [30]. Its function is similar to that of a histogram stretch but provides more consistent

results across a wider range of images [31]. The probability of gray level r_i in an image is defined by the equation:

$$p(r_i) = n_i / n \ (i=1, 2\ldots\ldots\ldots\ldots\ldots, L\text{-}1) \tag{3.1}$$

Where, L is the total number of possible gray levels in the researched image, n is the total number of pixels in the image, n_i is the number of pixels with gray level r_i. The cumulative distribution function (CDF) is used and can be expressed as

$$c_i = C(r_i) = \sum_{k=0}^{i} p(r_k) = \sum_{k=0}^{i} \frac{n_k}{n} \ (i=1, 2\ldots\ldots\ldots\ldots\ldots, L\text{-}1) \tag{3.2}$$

The inverse transformation from c to r can be used as below:

$$r_i = T^{-1}(c_i) \tag{3.3}$$

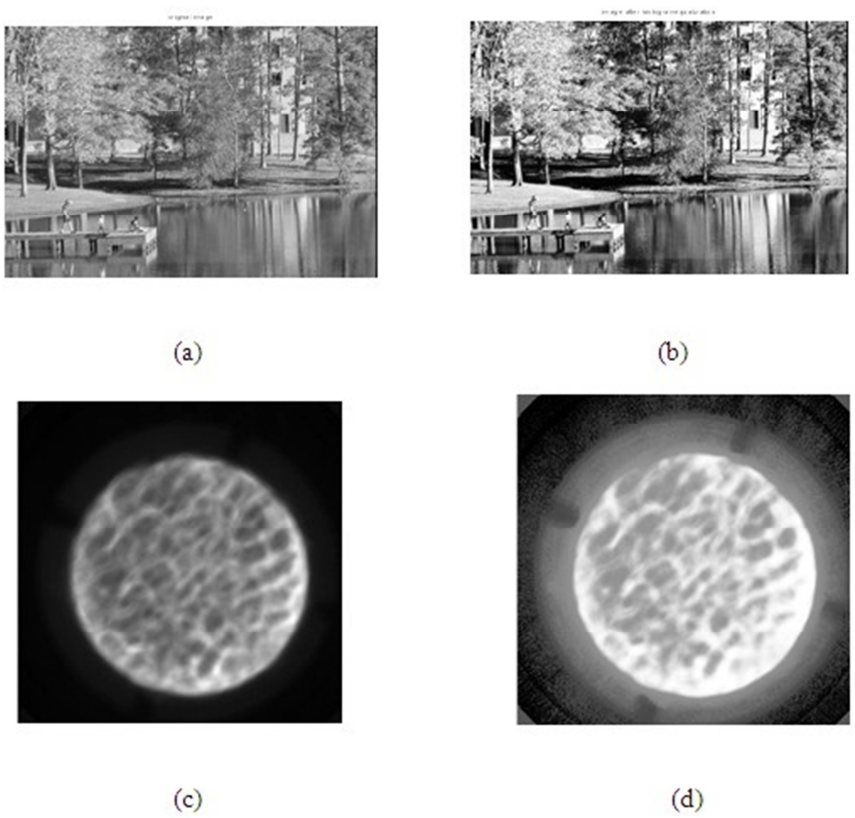

Figure 3.5 (a) Original image with lake and trees (b) image after histogram equalization (c) original 2D projection trabecular bone image (d) image after histogram equalization

3.4 Quantization

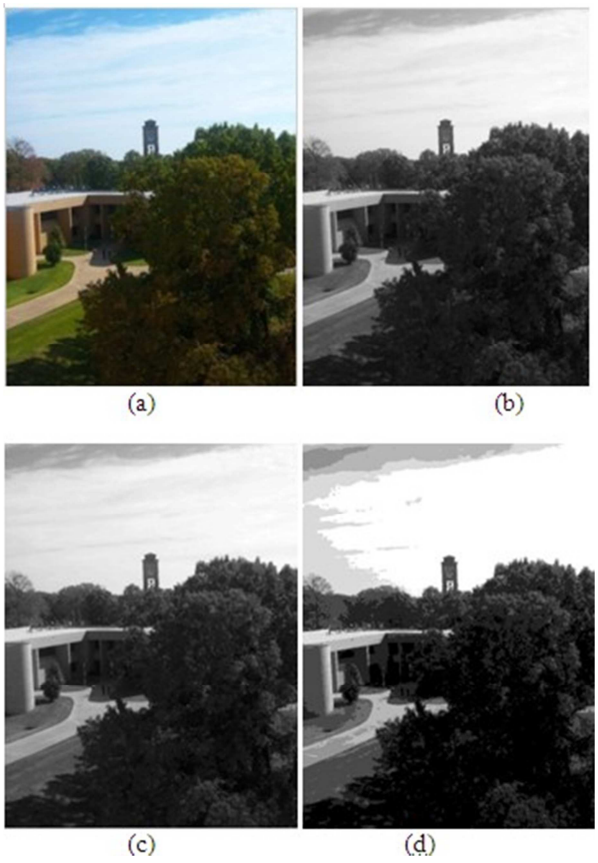

Figure 3.6 (a) Sample color image (b) gray scale image of sample with quantization level for 256 (c) gray scale image of sample with quantization level for 64 (d) gray scale image of sample with quantization level for 8

The number of gray levels is important as the matrix size depends on how many gray levels are present in the image. There is a tradeoff between the number of gray levels required for accurate description of textures and computational complexity. There are three major quantization schemes: (1) uniform quantization [32] (2) Gaussian quantization [33] and (3) equal probability quantization [3, 32]. The uniform quantization is the simplest and most popular form and is utilized for the bone images. The gray levels are quantized into separate bins with uniform tolerance limits or spaces. As defined below:

$$y = Q(x) \tag{3.4}$$

In function 3.4, y is the pixel value after quantization method, x is original pixel value. Q is the uniform quantization operation applied to image. It has been noted based on tests that eight gray levels are sufficient to derive textural properties.

Chapter Four

Experimental Procedure

Thirteen cylindrical specimens of cancellous bone from six males of different age ranges were used in this experiment. Some of them were normal bones and some were osteoporosis infested. Three crucial parameters were obtained from the mechanical tests on the bones: elastic modulus, strength; and bone volume fraction (BV/TV). These parameters play a key role in determining if a bone has been infested by osteoporosis. The image data and mechanical test data were provided by the Department of Health and Kinesiology, at The University of Texas at Tyler.

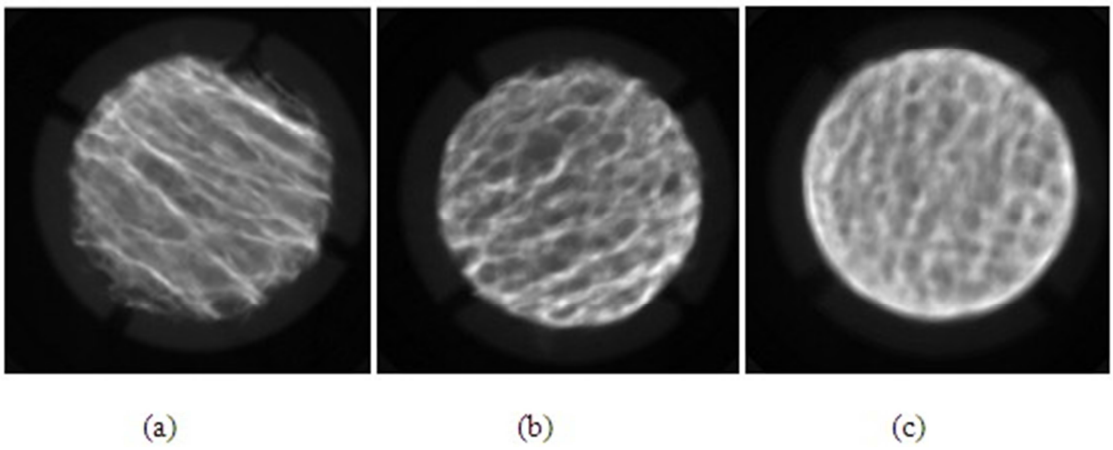

Figure 4.1 (a) 2D projection image of bone Strength for 0.73 Mpa (b) 2D projection image of bone Strength for 3.27 Mpa (c) 2D projection image of bone Strength for 8.42 Mpa

By averaging the gray values of the slice image from 3D image, 2D projection is obtained as shown in Figure 4.1. The resolution of the input image was 50 μm, generating an image of size 218 by 218 pixels in the objective image. In the 2D projection, the input image of the sample bone area needs to be separated from the

background. A thresholding method was used to figure out the edge of the bone. In further processing, blobs inside the circle were removed. The template binary image can be obtained as an index to the valid bone region.

Figure 4.2 shows a 2D image of trabecular bone with strength of 7.07 Mpa. After binary thresholding, an image which includes spots inside the circle is obtained. The dark spots are cleared with MATLAB function "*imfill*". The template image is used to localize the valid bone part being studied.

Figure 4.2 (a) Binary image with blobs (b) binary template (c) valid bone part extracted

If the histogram equalization was performed for the whole trabecular bone image, it would be affected adversely by the black background that occupies almost half of the entire image. The solution is to use the binary template image as an index to do the histogram equalization only on the valid bone and then obtain the enhanced picture on the spatial domain. See figure 4.3.

4.1 GLCM Computation

Some parameters are very important when computing the GLCM: number of quantization levels N_g; the displacement values *d*; the orientation value θ. Eight gray

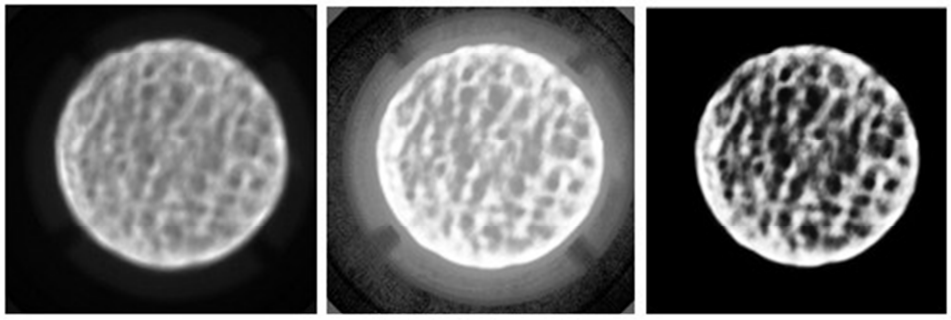

Figure 4.3 (a) Sample image with Strength for 8.42 Mpa (b) histogram equalization for the whole image (c) histogram equalization only on the valid bone part

levels were used in this experiment with the uniform quantization scheme to extract features from the 2D projection image. A displacement value d was set to 1, 2, 3, and 4 for every test image. The tested orientations were 0^{o}, 45°, 90°, 135°. Seven different GLCM features can be obtained from the experiment, namely; energy, contrast, autocorrelation, correlation, entropy, homogeneity; and cluster-shade. Hence for every tested image, 112 different data types corresponding to different orientations and displacement and features would be expected (Appendix B).

4.2 Semivariogram Analysis

Unlike the GLCM, where the matrix size was determined by the number of gray levels, the semivariogram ran on the whole image with 218*218 size. Quantization is not a factor for reducing calculation time. Also the histogram equalization is not required because of past experiments. However, the same ROI method is utilized and the displacement in the semivariogram will be set from 1 to 50. The orientations used are 0^{0}, 45^{0}, 90^{0}, 135^{0}. The values of the semivariogram are averaged. After getting 50 different semivariogram values, the obtained data is inserted into an exponential model to calculate

the nugget variance, sill and correlation length. Here the MATLAB function "*lsqcurvefit*", is used to provide us the best parameters for curve-fitting.

4.3 Statistical Analysis

How good one term is at predicting another is described by a standard parameter called the "Coefficient of Determination R^2". When the value of R^2 equals 1.0 and the value of one term are known, the value of another can be accurately predicted. That means these two terms are totally correlated. If R^2 is 0, knowing one term doesn't help predict another [34]. That means these two terms are totally uncorrelated. In general, a higher value of R^2 means that one term can be more accurately predicted from another.

The "Coefficient of Determination R^2" is often applicable in linear regression problems. Given a set of data points n, linear regression gives a formula for the line most closely matching those points [35]. It also gives a R^2 value to say how well the resulting line matches the original data points. The formula is:

$$R^2 = \left(\frac{n\sum_{i=1}^{n} x_i y_i - \left(\sum_{i=1}^{n} x_i\right)\left(\sum_{i=1}^{n} y_i\right)}{\sqrt{n\left(\sum_{i=1}^{n} x_i^{\,2}\right) - \left(\sum_{i=1}^{n} x_i\right)^2}\sqrt{n\left(\sum_{i=1}^{n} y_i^{\,2}\right) - \left(\sum_{i=1}^{n} y_i\right)^2}} \right) \tag{4.1}$$

In this project, after the data was obtained from the texture algorithm, the experimental data from the 2D projection image was correlated with the data obtained from the mechanical test. Linear regression methods were used to model the relationship between the mechanical test data (*y*) from 3D technique and experimental data (*x*) from the 2D projection image.

Chapter Five

Results

5.1 GLCM Feature Analysis Results

For each bone, the texture features extracted from the GLCM and semivariogram parameters were analyzed for a statistical fit with the mechanical test data. The mechanical testing indicated various levels of strength in trabecular bones: weak bone, medium bone, and strong bone. Orientation is very important for many of the GLCM parameters. The "Coefficient of Determination R^2" values were checked one by one for each parameter and each orientation (Appendix B). A sample analysis of results is shown below.

Table 5.1 Energy and Homogeneity for each bone sample (orientation for 0^0, displacement for 1)

Image Number	Elastic Modulus (MPa)	Energy	Homogeneity
1	126.0714	0.0662	0.8306
2	226.4135	0.0651	0.8269
3	119.7225	0.0647	0.8257
4	693.0832	0.0551	0.7757
5	552.2352	0.0674	0.8348
6	516.5530	0.0596	0.8010
7	427.3481	0.0595	0.7981
8	534.8067	0.0707	0.8532
9	1224.1589	0.0609	0.8095
10	1511.5544	0.0507	0.7496
11	1722.0936	0.0545	0.7696
12	1604.3418	0.0611	0.8064
13	1028.7697	0.0523	0.7576
R^2		0.395	0.401

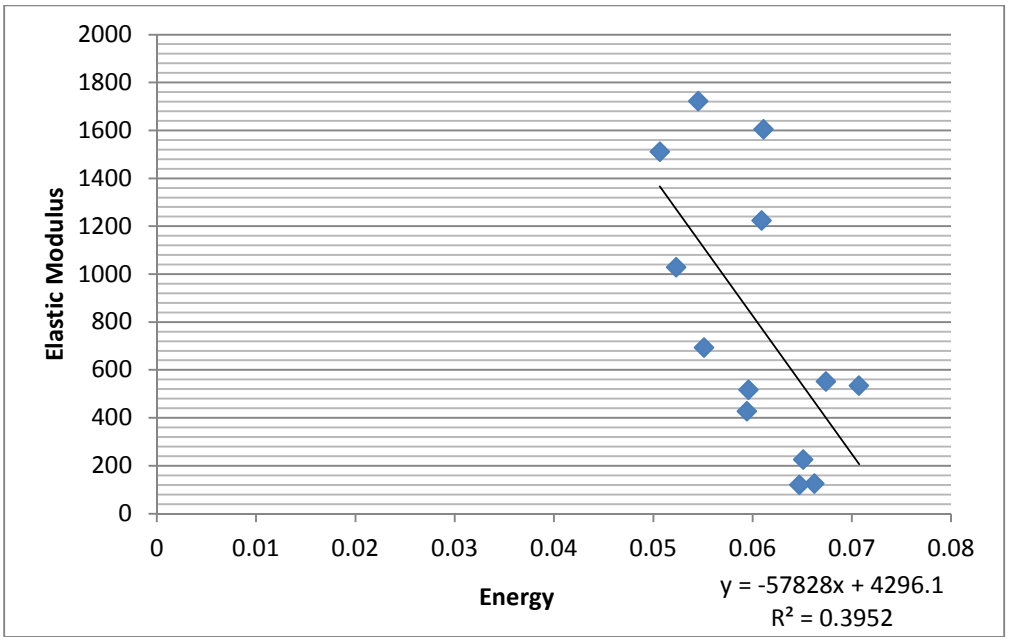

(a)

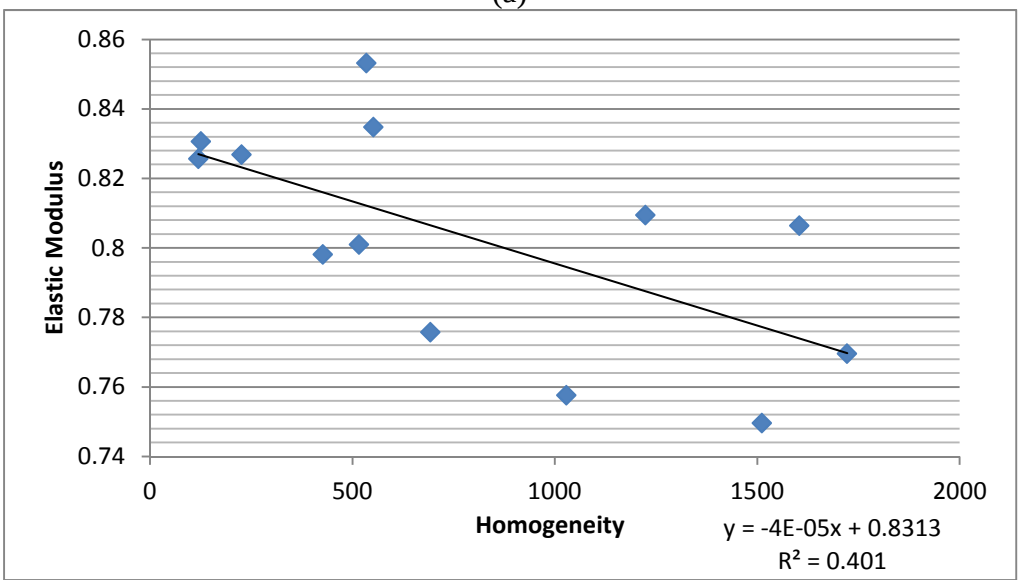

(b)

Figure 5.1 Linear regression models of Elastic Modulus (a) Energy with "Coefficient of Determination R^2" for 0.395 (b) Homogeneity with "Coefficient of Determination R^2" for 0.401

Table 5.1 and Figure 5.1 show us the correlation of energy and homogeneity to elastic modulus when orientation is 0^0, and displacement is 1. It can be concluded that these measures are only partially related with elastic modulus.

Table 5.2 "Coefficient of Determination R^2" values for different displacements for Energy, Entropy, Contrast, Homogeneity, Correlation and Autocorrelation with orientation for 0^0

R^2(Elastic Modulus)	d=1	d=2	d=3	d=4	Average
Energy	0.395	0.412	0.409	0.393	0.402
Entropy	0.45	0.45	0.447	0.434	0.445
Contrast	0.456	0.481	0.502	0.503	0.489
Homogeneity	0.401	0.41	0.424	0.429	0.416
Correlation	0.394	0.48	0.507	0.51	0.473
Autocorrelation	0.316	0.498	0.54	0.568	0.481

For example, it was observed that the parameters in Table 5.2 could somewhat predict the elastic modulus of the bone being tested.

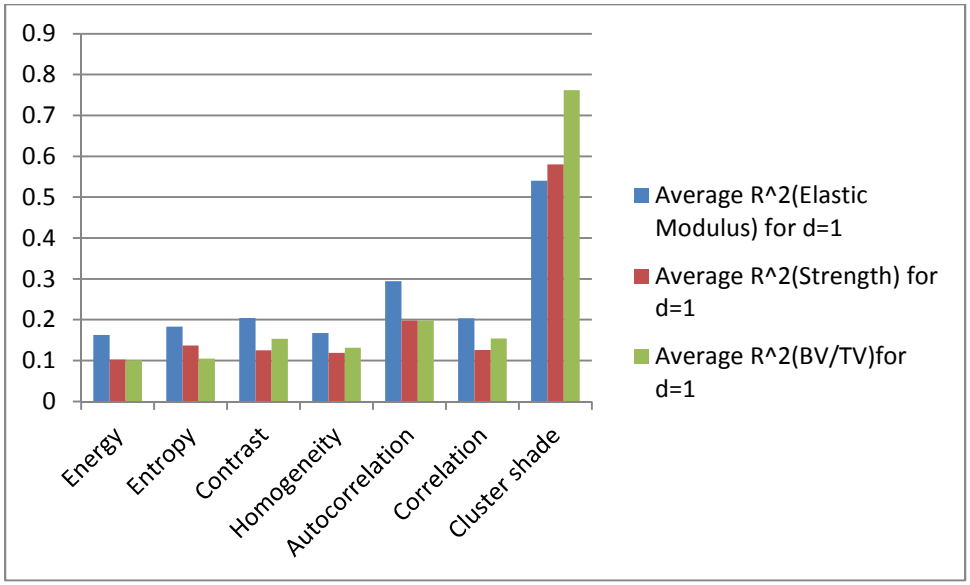

Figure 5.2 Four directions average R^2 value of every parameter when d=1

After thorough analysis of the results in Appendix B, the 'Cluster-Shade' parameter was found to correlate well in multiple orientations and distances when applied to all the feature parameters of the bone including the elastic modulus, strength, bone volume fraction (BV/TV), with especially strong fits with the BV/TV value. Figure 5.2 shows four direction's average R^2 value in linear regression model when displacement is

one, Figure 5.3 shows R^2 value between cluster shade and BV/TV when displacement is one and orientation is 0^0.

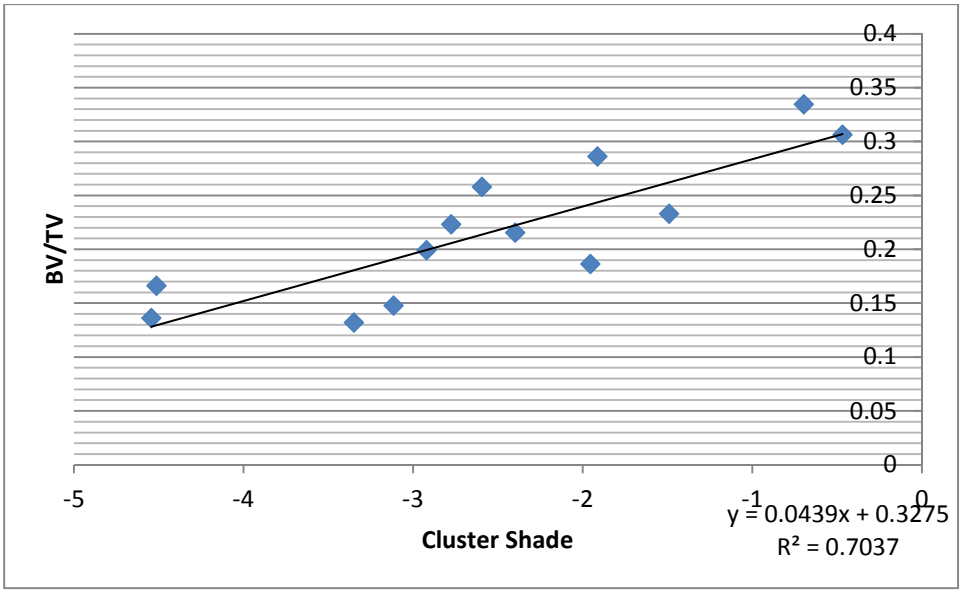

Figure 5.3 Linear regression models between Cluster Shade and BV/TV when d=2, orientation for 0^0

Table 5.3 Cluster Shade (*d*=2) corresponding to bone volume fraction (BV/TV) for different orientations

BV/TV	Cluster shade(0^0)	Cluster shade(45^0)	Cluster shade(90^0)	Cluster shade(135^0)
0.135896	-4.544	-6.491	-6.584	-7.418
0.147494	-3.115	-4.504	-4.893	-5.215
0.131742	-3.349	-9.268	-5.988	-3.345
0.16612	-4.513	-5.720	-5.820	-5.624
0.257839	-2.594	-0.732	-0.616	-0.325
0.186335	-1.954	-1.619	-2.618	-3.265
0.198986	-2.921	-3.537	-1.992	-2.450
0.223	-2.776	-3.184	-2.853	-3.092
0.21531	-2.397	-2.258	-2.179	-2.285
0.232785	-1.491	-1.032	-0.535	-1.522
0.334365	-0.697	-0.617	-1.285	0.643
0.306089	-0.468	-0.138	-0.421	0.661
0.286095	-1.912	-1.839	-1.860	-1.144
R^2	0.703	0.695	0.701	0.794

Table 5.4 Elastic Modulus fit with Cluster Shade for various displacements and orientations

R^2(Elastic Modulus)	d=1	d=2	d=3	d=4
0^0	0.336	0.647	0.687	0.68
45^0	0.571	0.542	0.478	0.445
90^0	0.442	0.521	0.501	0.447
135^0	0.422	0.544	0.571	0.552
average	0.442	0.564	0.557	0.531

From Table 5.4, it can be observed that the orientation also plays a very important role when fitted with data between the elastic modulus and cluster shade, especially when the displacement is set to 2, 3, 4 at 0^0. The values indicate that a higher cluster shade value means a stronger bone.

Table 5.5 Bone Strength fit with Cluster Shade for various displacements and orientations

R^2(Strength)	d=1	d=2	d=3	d=4
0^0	0.316	0.678	0.728	0.706
45^0	0.58	0.583	0.519	0.478
90^0	0.433	0.569	0.565	0.541
135^0	0.436	0.6	0.624	0.588
average	0.441	0.608	0.609	0.578

From Table5.5, it can be safely concluded that Cluster Shade correlated well with bone strength.

Table 5.6 BV/TV fit with Cluster Shade for various displacements and orientations

R^2(BV/TV)	d=1	d=2	d=3	d=4
0^0	0.26	0.703	0.855	0.879
45^0	0.609	0.695	0.655	0.628
90^0	0.43	0.701	0.733	0.704
135^0	0.46	0.794	0.852	0.838
average	0.44	0.723	0.774	0.762

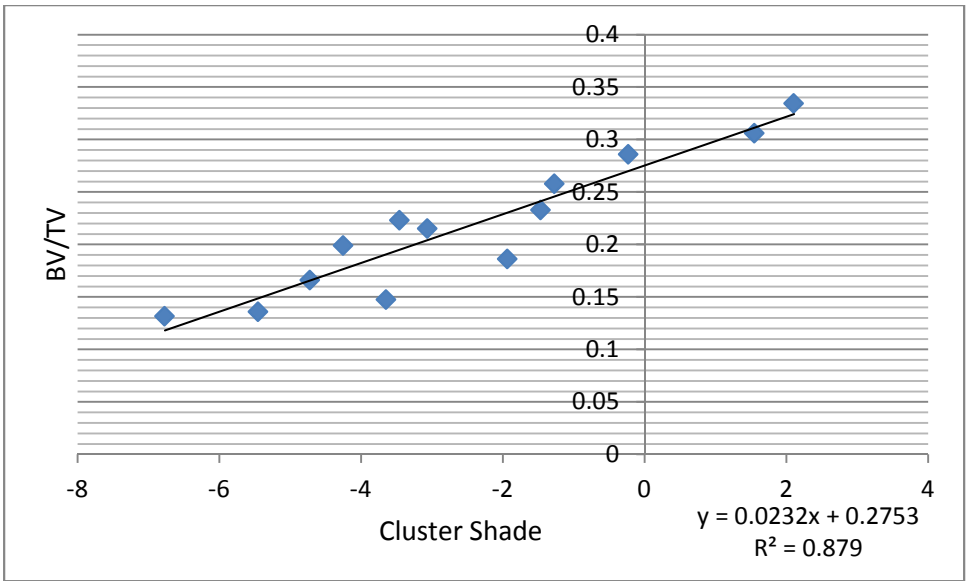

Figure 5.4 The highest "Coefficient of Determination R^2" in Cluster Shade and BV/TV

From Table 5.6, according to the value of "Coefficient of Determination R^2", this data set fits very well with BV/TV. The highest value equals 0.879 (d=4, orientation for 0^0).

According to the regression analysis done earlier for every parameter, it can be seen that the cluster shade is the best parameter from GLCM features to use in predicting bone features.

5.2 Semivariogram Analysis Results

The value of the semivariogram increases with the displacement *d* if the image pixels are spatially correlated. The reason is that pixels located closer to each other tend to be more similar than pixels located farther from each other. However, in most cases, it will reach a peak at certain displacement values. The texture features are based on this displacement variety [36].

This variety behavior was validated by the analysis, with the region of interest covering the whole bone (not just part of area taken from bone). The semivariogram in the 2D projection image with a low strength reached its lower maximum value, and reached the peak slowly (Figure 5.5). However, the ones with higher strength have higher maximum semivariogram value and arrive at the plateau more rapidly (Figure 5.6).

The semivariogram has been proven to identify a strong or a weak bone [16]. In this project, this method is applied to the same bone data samples used for the GLCM based analysis.

Table 5.7 Different "sill" values corresponding to Elastic Modulus, Strength, and BV/TV

Elastic Modulus (MPa)	Strength (MPa)	BV/TV	Sill
126.0714288	0.89872794	0.135896	2469
226.4135295	1.317838342	0.147494	2993
119.7225897	0.736991678	0.131742	3300
693.0832725	3.574800483	0.16612	8962
552.23525	3.936745717	0.257839	6228
516.553024	3.278947907	0.186335	6913
427.3481559	2.892875023	0.198986	3383
534.8066583	3.625236217	0.223	3416
1224.158963	7.581007434	0.21531	9526
1511.554474	7.072443151	0.232785	9754
1722.093557	8.427645863	0.334365	10352
1604.341796	11.71234862	0.306089	11098
1028.769721	6.49845677	0.286095	7300

Table 5.7 shows the "sill" value and is computed with sample data. Figure 5.7 shows linear regression model analysis for each parameter. As we observed from Table 5.7 and Figure 5.7, the semivariogram's "sill" value fits very well with the strength and elastic modulus, however fits relatively poorly with the BV/TV.

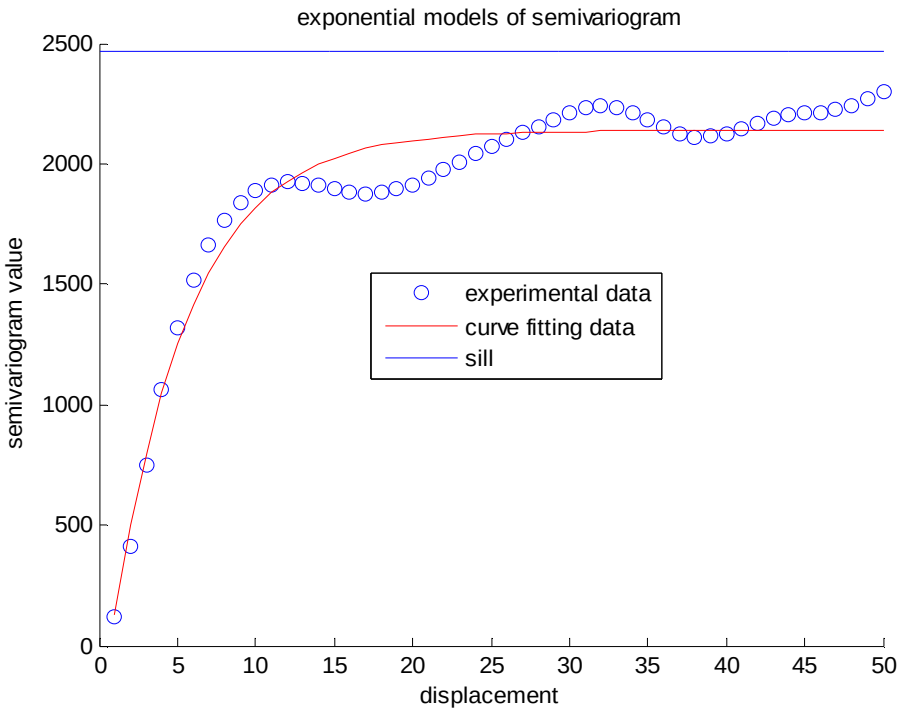

Figure.5.5 Weak bone with Strength for 0.9 Mpa, in the exponential model (sill for 2469)

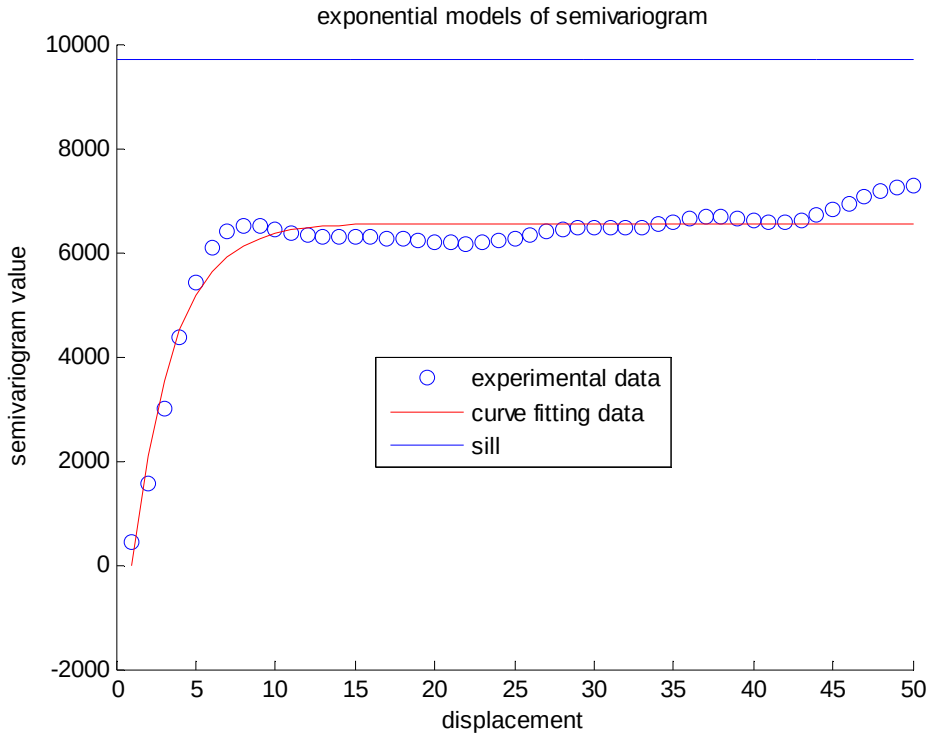

Figure 5.6 Strong bone with Strength for 7.07 Mpa in the exponential model (sill for 9754)

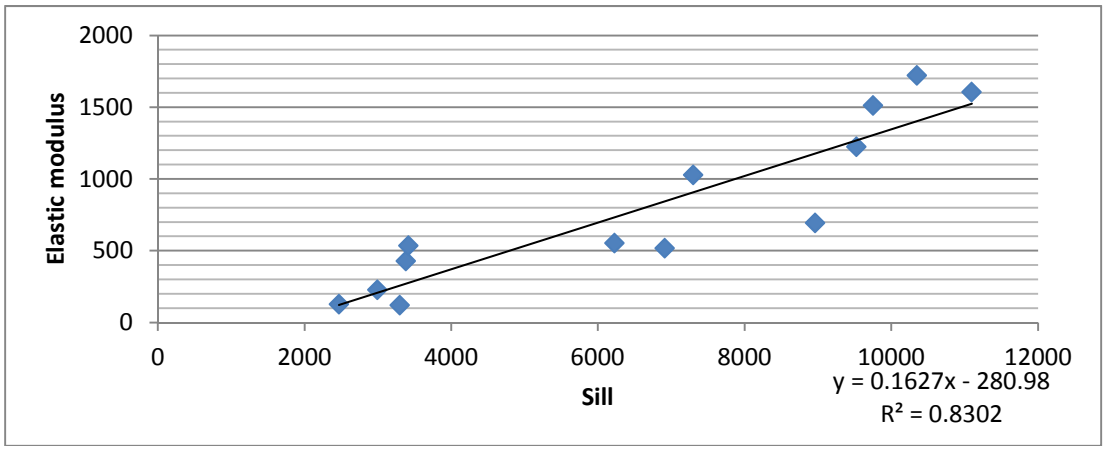

(a)

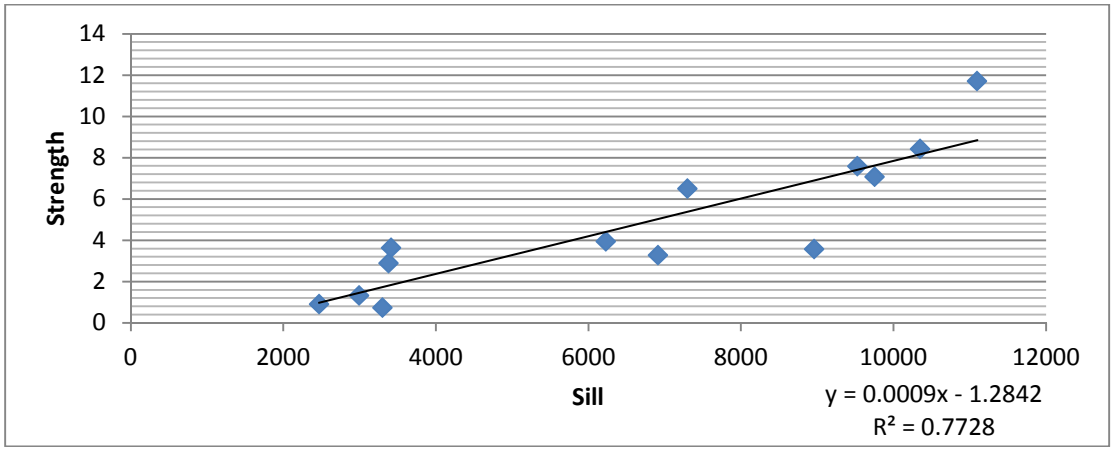

(b)

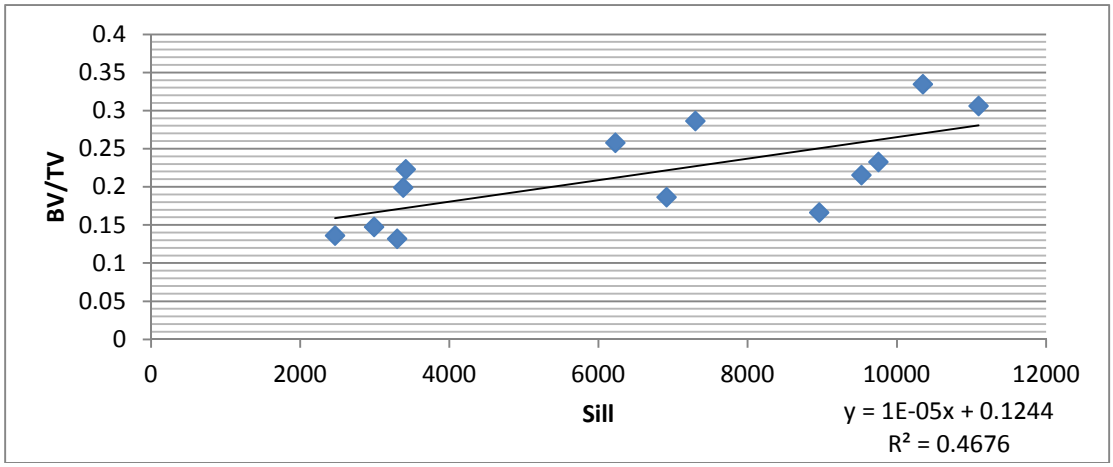

(c)

Figure 5.7 Linear regression model applied to (a) Elastic Modulus and “sill” (b) Strength and “sill” (c) BV/TV and “sill”

Chapter Six

Discussion and Conclusion

The results from GLCM feature analysis demonstrate that it is possible to estimate bone's textural features, microstructure and mechanical properties with the GLCM parameter called 'Cluster Shade'. The linear regression testing with ground truth data from bone samples showed a high "Coefficient of Determination R^2" value, and fits well with one of the bone's most important microstructure parameters called BV/TV. It was also noted the features of the bone may be derived from other GLCM features such as energy, entropy, contrast, homogeneity, correlation autocorrelation, and elastic modulus in some displacements and orientations.

1233	265	97	76	65	60	39	14
380	552	404	316	256	188	108	82
127	467	574	422	371	281	184	163
61	370	400	322	357	362	239	193
36	284	384	338	364	406	372	295
27	200	373	352	428	439	382	434
20	94	218	253	331	432	489	577
14	43	127	214	301	461	598	837

Figure 6.1 GLCM matrix bone with low Strength for 0.9 Mpa (displacement for 4, quantization levels for 8, orientation for 90^0)

Cluster shade relies on the directional means of the GLCM. In most of our experiments eight quantization levels were utilized and the means of the two dimensional projection image of the GLCM lies between 4 and 5. This parameter defines 'imaginary symmetric lines' from the top right corner to lower left corner. Elements located further from these 'imaginary symmetric lines' play more important roles in the textural features or symmetric properties of the bone.

In figure 6.1, the sum of $\mu_{x,}\mu_{Y}$ equals 9.32. Because of this, the 'imaginary symmetric lines (red line) are located a little closer to lower left corner. The first point (the red circle) which is also the farthest point plays the most important role in the cluster shade of this matrix and leads the value of total cluster shade to -10.27. Generally, if more shades appear in the top left corner, the cluster shade value will be more negative. Relatively, the lower right corner tends to be more positive. This may be the reason why cluster shade fits better with bone images than other parameters obtained from the GLCM matrix, because other parameters are positive. Also, more quantization levels provide larger absolute values of cluster shade. Cluster shade also depends on the “spread” of the matrix value away from the diagonal. From this project, assumption can be made that behavior of this “spread” of GLCM matrix highly correlates to real world bone’s micro-architectural properties.

In most cases, pixels located closer to each other are more similar than pixels located farther apart. This phenomenon agrees with the semivariogram because its value increases as *h* increases. This anticipated behavior is similar to the texture feature of ‘Contrast’ in GLCM. Also, higher semivariogram values correspond to lower ‘Correlation’ values because the ‘Correlation’ indicates the coefficient of the two observed variables *i* and *j* in the GLCM. From this experiment, even the semivariogram can’t fit very well with bone volume fraction, it shows a better linear regression “Coefficient of Determination R^2 ” value with strength and elastic models.

Finally, comparing the two methods, cluster shade from GLCM provides an excellent fit with bone volume fraction data, which is our first purpose to detect

microstructure of bone. However, the “sill” recovered from semivariogram gives a better method to prediction of the strength and elastic modulus of bone.

6.1 Future Work

There is still a lot to explore using the commonly used parameters of GLCM. For example, we could use different quantization methods such as “equal probability” as Hararick described in his paper [3], or the number of quantization levels can be increased. Other texture algorithms deserve for the study in 2D projection bone images, for example, gray-level difference vector [18], max-min texture [19], Fourier power spectrum [22].

In addition, trabecular bone samples in this project were taken from six human subjects, so the sampling may not be enough to have a significant conclusion. More samples from more human subjects should be studied in the near future.

Moreover, for the semivariogram, histogram equalization was not used. Histogram equalization proved to be a good method to enhance spatial-relationships. Different quantization levels to reduce calculation time can also be investigated.

6.2 Conclusion

This study has described the implementation of texture algorithms based on Gray level co-occurrence matrices and semivariograms. Parameters selected from these algorithms reveal its relationship with a bone’s microstructure and mechanical properties. The GLCM based cluster shade proved to be an effective method of predicting three dimensional bone’s microstructure from two dimensional projection images. The

semivariogram based “sill” gives an excellent prediction method for mechanical properties of bones. Discovering these methods is very important because it provides a very convenient and economic solution to predicting bone quality for medical applications such as osteoporosis.

References

[1] M. Haralick, K. Shanmugam and I. Dinstein, "Textural features for image classification," *IEEE Transactions* on *Systems*, vol. 3, no. 6, pp. 610-621, 1973.

[2] M. Haralick, "Statistical and structural approaches to texture," *Proceedings of* the *IEEE*, vol. 67, no. 5, pp. 786–804, 1979.

[3] C. H. Turner, J. Y. Rho, R. B. Ashman, and S. C. Cowin, "The dependence of elastic constants of cancellous bone upon structural density and fabric," *The 47th Annual Meeting* of *Orthopaedic Research Society*, (February 1998), pp. 13-74.

[4] G. Luo, J. H. Kinney, J. J. Kaufman, and D. Haupt, "Relationship between plain radiographic patterns and three dimensional trabecular architecture in the human calcaneus," *Osteoporosis International*, vol. 9, no. 7, pp. 339–345, 1999.

[5] C. L. Benhamou, E. Lespessailles, G. Jacquet, R. Harba, and R. Jennane, "Fractal organization of trabecular bone images on calcaneus radiographs," *Journal of Bone and Mineral Research* vol. 9, no. 12, pp. 1109 –1118, 2009.

[6] J. C. Buckland-Wright, J. A. Lynch, and D. G. Macfarlane, "Fractal signature analysis measures cancellous bone organization in macroradiographs of patients with knee osteoarthritis," *Annals of the Rheumatic Diseases*, vol. 55, no. 10, pp. 749 –755, 1996.

[7] D. Chappard, A. Chennebault, M. Moreau, and E. Legrand , "Texture analysis of x-ray radiographs is a more reliable descriptor of bone loss than mineral content in a rat model of localized disuse induced by the clostridium botulinum," *Toxin Bone*, vol. 28, no. 1, pp. 72-79, 2001.

[8] L. K. Soh, and C. Tsatsoulis, "Texture analysis of SAR sea ice imagery using gray level co-occurrence matrices," *Geoscience* & *Remote Sensing*, vol.37, no. 2, pp. 150-161, 1999.

[9] Q. A. Holmes, D. R. Nuesch, and R. A. Shuchman, "Textural analysis and real-time classification of sea-ice types using digital SAR data," *Geoscience* & *Remote Sensing*, vol. 22, pp. 113–120, 1984.

[10] S.Y. Hsu, "Texture-tone analysis for automated land-use mapping," *Photogrammetric Engineering & Remote Sensing*, vol. 44, no. 11, pp. 1393–1404, 1978.

[11] E. Ebert, "A pattern recognition technique for distinguishing surface and cloud types in the polar regions," *Journal of Climate and Applied Meteorology*, vol. 26, no. 10, pp. 1412–1427, 1987.

[12] L. Garand, "Automated recognition of oceanic cloud patterns, Methodology and application to cloud climatology," *Journal of Climate,* vol. 1, no. 1 pp. 20–39, 1988.

[13] A. Mcbratney, and R. Webster,"Choosing functions for semi-variograms of soil properties and fitting them to sampling estimates," *Journal* of *Soil Science*, vol. 37, no. 4, pp. 617-639, 1986.

[14] P. M. Atkinson, and C. D. Lloyd, "Non-stationary variogram models for geostatistical sampling optimisation: an empirical investigation using elevation data," *Computers & Geosciences*, vol. 33, no. 10, pp. 1285–300, 2007.

[15] R. Webster and M. A. Oliver, *Geostatistics for environmental scientists/2nd edition*, Hoboken, NJ: John Wiley & Sons, 2007.

[16] X. D. Dong, "Random field assessment of nanoscopic inhomogeneity of bone" *Bone*, vol. 47, no, 6, pp. 1080-1084, 2010.

[17] M. Galloway, "Texture analysis using gray level run lengths," *Computer Graphics and Image Processing*, vol. 4, no. 2, pp. 172–179, 1975.

[18] J. S. Weszka, C. R. Dyer, and A. Rosenfeld, "A comparative study of texture measures for terrain classification," *IEEE Transactions on Systems, Man, and Cybernetics*, vol. 6, no. 4, pp. 269–285, 1976.

[19] O. R. Mitchell, C. R. Myers, and W. Boyne, "A max–min measure for image texture analysis," *IEEE Transactions on Computers*, vol. 26, no. 4, pp. 408–414, 1977.

[20] M. Unser, "Sum and difference histograms for texture classification," *Pattern Analysis and Machine Intelligence*, vol. 8, no. 1, pp. 118–125, 1986.

[21] L. Wang and D. C. He, "A new statistical approach for texture analysis," *Photogrammetric Engineering* &*Remote Sensing*, vol. 56, no. 2, pp. 61–66, 1990.

[22] G. O. Lendaris and G. L. Stanley, "Diffraction pattern sampling for automatic pattern recognition," *Proceedings of the IEEE*, vol. 58, no. 2, pp. 198–216, 1970.

[23] *B. Julesz*, "Binocular depth perception without familiarity cues," *Science, New Series*, vol. 145, no. 3, pp. 356-362, 1964.

[24] X. Wang, R. R. Zauel, D. S. Rao, and D. P. Fyhrie, "Cancellous bone lamellae strongly affect microcrack propagation and apparent mechanical properties: separation of patients with osteoporotic fracture from normal controls using a 2D nonlinear finite element method (biomechanical stereology)," *Bone*, vol. 42, no. 6, pp. 1184–1192, 2008.

[25] R. W. Conners, and T. Trivedi “Segmentation of a high-resolution urban scene using texture operators,” *Computer Vision, Graphics, and Image Processing*, vol. 25, no. 3, pp. 273-310, 1984.

[26] N. Ravia Shabnam, M. Parveen, M. Phil “Enhancement of bone fracture images by equalization methods” *International Conference on Computer Technology and Development*, (Kota Kinabalu, Nov 13-15, 2009), pp. 391-394.

[27] S. Mehmet, “Survey over image thresholding techniques and quantitative performance evaluation,” *Journal of Electronic Imaging*, vol. 13, no. 1, pp. 146–165, 2004.

[28] J. Serra, *Image Analysis and Mathematical Morphology*, Academic Press, 1998.

[29] E. R. Dougherty, *An Introduction to Morphological Image Processing*, SPIE-International Society for Optical Engine, 1992.

[30] T. Acharya and A. K. Ray, *Image Processing: Principles and Applications*, Hoboken, NJ: Wiley-Interscience, 2005.

[31] R. C. Gonzalez, and R. E. Woods, *Digital Image Processing*, Upper Saddle River, NJ: Prentice Hall, 2002.

[32] A. Gersho, “Asymptotically optimal block quantization,” *IEEE Information Theory Society*, vol. 25, no. 4, pp. 373–380, 1979.

[33] R.M. Gray and D.L. Neuhoff, “Quantization,” *IEEE Transactions on Information Theory*, vol. 44, no. 6, pp. 2325–2384, 1998.

[34] N. R. Draper, *Applied Regression Analysis*, Hoboken, NJ: Wiley-Interscience, 1998.

[35] N. Nagelkerke, J. D. *Maximum Likelihood Estimation of Functional Relationships (Lecture Notes in Statistics)*, New York, NY: Springer, 1992.

[36] Chiles, Delfiner, 1999, *Geostatististics, Modelling Spatial Uncertainty*, Hoboken, NJ: Wiley-Interscience, 1999.

Appendix A

MATLAB Code

```
%%%%%%%%%%%%%%%%%%main code of GLCM%%%%%%%%%%%%%%%%%%%%%%%%%%%%%%%%%%%%%%%%
clc
%because of some images in the beginning and the end are invalid
%so we take image from 15 to 200.
zmin=15;zmax=200;
%function "readimage" read 2d projection image from 3D dicom picture
[P]=readimage(zmin,zmax);
% convert to integer range 0-255
g=mat2gray(P);
P=im2uint8(g);
g=P;
L=input('L=');%L=45;main threshold gray level is 45.
%make a new binary image as index,inner part is valide bone part.outer
%is background which we don't need.
%function "circletemplate" create circle template: g
[g]=circletemplate(P,g,L);
% "histeqtry" is the histogramequalizaion only in the inner part.
P=histeqtry(P,g);
%figure,imshow(P),impixelinfo %figure
Q=input('Q=');%Q=8; number of gray level value in GLCM, we use 8
%Quantization number of gray level
H=fix(double(P)/(256/Q));
%figure,imshow(H,[]),impixelinfo
%glcmfour:calculateglcm in four direction p1=0degree, p2=45
%degree,p3=90degree,p4=135 degree
d=input('d=');%d=1,2,3,4 in our project
[p1,p2,p3,p4]=glcmfour(H,g,Q,d);
%"glcmparameter" calculate 7 different parameters of GLCM
glcmparameter(p1,p2,p3,p4,Q);
```

```
%%%%%%%%%%%%%%%%%%function of readimage%%%%%%%%%%%%%%%%%%%%%%%%%%%%%%%%%%%%%
function [P]=readimage(m,n)
%read micro-CT images with DICOM format and store them
root='export';
start=m;
inte=1;
last=n;
num=start:inte:last;
ii=0;
num

%create an empty array
Projection2D = zeros(218,218,'double');
forifile=num;
    ii=ii+1;
    n4='0000';n4(4-length (num2str(ifile))+1:4)=num2str(ifile);
```

Appendix A (continued)

```
    name=[root '-' n4 '.dcm'];
if exist(name)
fprintf('-------Reading images files %s ---------\n', name);
microCTSlice = dicomread(name);
end
Projection2D=Projection2D+double(microCTSlice);
end;

%take the average of grey values
P=Projection2D/(n-m+1);



%%%%%%%%%%%%%%%%%%function circletemplate%%%%%%%%%%%%%%%%%%%%%%%%%%%%%%%%
%In this function we create binary image as index of valid bone
%because there may be some dark part inside the circle, we must delete
it

function [g]=circletemplate(P,g,L)

%figure,imshow(P),impixelinfo

[M,N] = size(P);
for i=1:M
for j=1:N
if P(i,j)<L
                    g(i,j)=0;
else
                    g(i,j)=1;
end
end
end

    g = imfill(g, 'holes');
%figure,imshow(g),impixelinfo


%%%%%%%%%%%%%%%%%function histeqtry%%%%%%%%%%%%%%%%%%%%%%%%%%%%%%%%%%%%%%%
%this is function of the histogramequalizaion only in interest part of
%the picture, input x means the original picture, g is template
%image that we check the valid part, y is the output picture after
%histogramequalizaion in the valid part

function y=histeqtry(x,g)

[M,N] = size(x);
P=zeros(1,256);%create an zero array with 256 element

for i=1:M
for j=1:N
if g(i,j)==1 % check the circletemplate
             k=x(i,j);   %k is pixel value
```

Appendix A (continued)

```
            P(k+1)=P(k+1)+1;

end
end
end

     P=P/sum(P); %the probability of every pixel value in the inner
part
%    figure,bar(0:255,P,'g')
%Cumulative of probability of every pixel value in the inner part

 S1=zeros(1,256);
for i=1:256
for j=1:i
          S1(i)=P(j)+S1(i);
end
end

S2=round((S1*256)-0.5);
figure,bar(0:255,S2,'g')
y=x;
%after rearrange the pixel value in the inner part, we got the
%histogramequalizaion picture only in the innerpart.S2 become the index
%value of new histogramequalizaion image
for i=1:M
for j=1:N
if g(i,j)==1
               k=x(i,j);
     y(i,j)=S2(k+1);  %put the new pixel value into new picture
end
end
end
%figure,imshow(y),impixelinfo



%%%%%%%%%%%%%%%%%function glcmfour%%%%%%%%%%%%%%%%%%%%%%%%%%%%%%%%%%%%%%
% H is 2d projection image,A is template image, L is number of gray
%level which also determine the size of GLCM.

function [p1,p2,p3,p4]=glcmfour(H,A,L,d)
[M,N]=size(H);
P=zeros(L,L,4);%different degree.
k=d-1;

for i=1:M
for j=1:N
if j<N-k&&A(i,j)>0&&A(i,j+d)>0    %zero degree
                    l1=H(i,j)+1;      %for the difference first index
                    l2=H(i,j+d)+1;%between GLCM matrix and real picture
                    P(l1,l2,1)=P(l1,l2,1)+1;
```

Appendix A (continued)

```
End
if i>d&&j<N-k&&A(i,j)>0&&A(i-d,j+d)>0 %45 degree
                    l1=H(i,j)+1;
                    l2=H(i-d,j+d)+1;
                    P(l1,l2,2)=P(l1,l2,2)+1;


end
if i<M-k&&A(i,j)>0&&A(i+d,j)>0     %90 degree
                    l1=H(i,j)+1;
                    l2=H(i+d,j)+1;
                    P(l1,l2,3)=P(l1,l2,3)+1;


end
if i<M-k&&j<N-k&&A(i,j)>0&&A(i+d,j+d)>0 %135 degree
               l1=H(i,j)+1;
               l2= H(i+d,j+d)+1;

                    P(l1,l2,4)=P(l1,l2,4)+1;

end
end
end

P(:,:,1)
P(:,:,2)
P(:,:,3)
P(:,:,4)

for n = 1:4
    P(:,:,n) = P(:,:,n)/sum(sum(P(:,:,n))); %normalize
end
p1=P(:,:,1);%0  degree GLCM matrix
p2=P(:,:,2);%45 degree GLCM matrix
p3=P(:,:,3);%90 degree GLCM matrix
p4=P(:,:,4);%135 degree GLCM matrix



%%%%%%%%%%%%%%%function glcmparameter%%%%%%%%%%%%%%%%%%%%%%%%%%%%%%%%%%%%
%In this function we calculate each parameters of GLCM, They are
%energy, entropy, contrast, correlation, homogeniety, cluster shade
Function glcmparameter(p1,p2,p3,p4,L)

P(:,:,1)=p1;
P(:,:,2)=p2;
P(:,:,3)=p3;
P(:,:,4)=p4;

F = zeros(1,4);
A = F;
```

Appendix A (continued)

```
E=F;
Ux = F;      Uy = F;
deltaX= F;  deltaY = F;
C =F;
H= F;
S =F;
U=F;
R=F;
for n=1:4

A(n) = sum(sum(P(:,:,n).^2)); %energy(angular second moment)
for l1 = 1:L
for l2 = 1:L
if P(l1,l2,n)~=0
                E(n) = -P(l1,l2,n)*log(P(l1,l2,n))+E(n); %entropy
end

            C(n) = (l1-l2)^2*P(l1,l2,n)+C(n);  %contrast

            H(n)=P(l1,l2,n)/(1+(l1-l2)^2)+H(n);% local homogenity

Ux(n) = l1*P(l1,l2,n)+Ux(n); %¦Ìx
Uy(n) = l2*P(l1,l2,n)+Uy(n); %¦Ìy

end
end
end
for n=1:4
for l1 = 1:L
for l2 = 1:L
            S(n)=P(l1,l2,n)*((l1+l2-Ux(n)-Uy(n))^3)+S(n);%cluster shade

deltaX(n) = (l1-Ux(n))^2*P(l1,l2,n)+deltaX(n); %¦Òx
deltaY(n) = (l2-Uy(n))^2*P(l1,l2,n)+deltaY(n); %¦Òy
            R(n) = l1*l2*P(l1,l2,n)+R(n);
            U(n) = l1*l2*P(l1,l2,n)+U(n); %Auto-correlation
end
end
    R(n) = (R(n)-Ux(n)*Uy(n))/deltaX(n)/deltaY(n);      %corelation
end

%figure of the each parameter in different direction.
figure;
subplot(4,2,1);stem(A,'filled');title('Energy');
subplot(4,2,2);stem(E);title('Entropy');
subplot(4,2,3);stem(C,'c');title('Contrast');
subplot(4,2,4);stem(H,'.');title('homogeniety');
subplot(4,2,5);stem(S,'o');title('cluster shade');
subplot(4,2,6);stem(R,'*');title('Correlation');
subplot(4,2,7);stem(U,'^');title('Autocorrelation');

%put the data into excel
xlswrite('his132.xls',A,1,'A1:D1')
```

Appendix A (continued)

```
xlswrite('his132.xls',E,1,'E1:H1')
xlswrite('his132.xls',C,1,'I1:L1')
xlswrite('his132.xls',H,1,'M1:P1')
xlswrite('his132.xls',S,1,'Q1:T1')
xlswrite('his132.xls',R,1,'U1:X1')
xlswrite('his132.xls',U,1,'Y1:AB1')


%%%%%%%%%%%%%%%%%main function of semivariogram%%%%%%%%%%%%%%%%%%%%%%%%%
% get semivariogram value, the displacement set to 50
%obtain inputs from users

zmin=15;zmax=200;
%read 2D image from 3D image
[P]=readimage(zmin,zmax);

P=int16(P);
P=fix(double(P));
figure,imshow(P,[]),impixelinfo
g=P;
L=210;%L=input('L=');% we take out the eadge by the threholding method
[g]=circletemplate(P,g,L);% we only consider ROI part of image
figure,imshow(g,[]),impixelinfo

d=input('d=');%d=50-distance between two observed pair, use 50 in here
G=zeros(1,d);
%calculate different semivariogram when h increase
for k=1:d
    [s]=newvar(g,P,k);
    G(k)=s;

end

%figure,scatter(1:75,G,'g')
T=zeros(1,d);
for k=1:d
    T(k)=k;
end

x=T;
y=G;
%use curfit mesthod to calculate semivarogram value.
initialConditions = [-110 8000 10];%the initial conditions according to
%estimate of start point of function
[newParameters,error] = lsqcurvefit(@myPolyCurve,
initialConditions,x,y);

figure
scatter(x,y) %plot the scatter plot
```

Appendix A (continued)

```
hold %hold the figure
newParameters
%use new parameters to get new output values
y2 = myPolyCurve(newParameters,x);
%plot the new data using the read color
plot(x,y2,'r')
title('exponential models of semivariogram')
xlabel('displacement')
ylabel('semivariogram value')


%%%%%%%%%%%%%%%%%%%%function newvar%%%%%%%%%%%%%%%%%%%%%%%%%%%%%%%%%%%%%%%%
%calculate semivariogram in each direction,only in ROI part

function [S]=newvar(g,P,d)

h=zeros(1,4);
p=zeros(1,4);
G=zeros(1,4);
[M,N]=size(P);
%-------------------------------------
for i=1:M %0degree
for j=1:N-d

if g(i,j)>0&&g(i,j+d)>0

                l1=(P(i,j)-P(i,j+d))^2;
                p(1)=p(1)+1;%calculate how many pairs they runs.
                h(1)=h(1)+l1;%sum of semivariogram

end
end
end
G(1)=h(1)/(2*p(1));
%-------------------------------------
for i=(d+1):M %45degree
for j=1:N-d

if g(i,j)>0&&g(i-d,j+d)>0

                l2=(P(i,j)-P(i-d,j+d))^2;
                p(2)=p(2)+1;%calculate how many pairs in this algorithm
                h(2)=h(2)+l2;%sum of semivariogram

end
end
end
G(2)=h(2)/(2*p(2));
%-------------------------------------
for i=1:M-d %90degree
for j=1:N
if g(i,j)>0&&g(i+d,j)>0
```

```
                l3=(P(i,j)-P(i+d,j))^2;
                p(3)=p(3)+1;%calculate how many pairs they runs.
                h(3)=h(3)+l3;%sum of semivariogram

end
end
end
G(3)=h(3)/(2*p(3));
%---------------------------------------
for i=1:M-d %135degree
for j=1:N-d

if g(i,j)>0&&g(i+d,j+d)>0

                l4=(P(i,j)-P(i+d,j+d))^2;
                p(4)=p(4)+1;%calculate how many pairs they runs.
                h(4)=h(4)+l4;%sum of semivariogram

end
end
end
G(4)=h(4)/(2*p(4));
%take the average of every direction.
S=sum(G)/4;



%%%%%%%%%%%%%%%function mypolycurve%%%%%%%%%%%%%%%%%%%%%%%%%%%%%%%%%%%%%%%%%%%
function output= myPolyCurve (param,input)
a = param(1);
b = param(2);
c=  param(3);

% this is the 3rd order polynomial equation here

output = a+b*(1-exp(-input/c));
```

Appendix B

Bone Properties Corresponding to GLCM Parameters

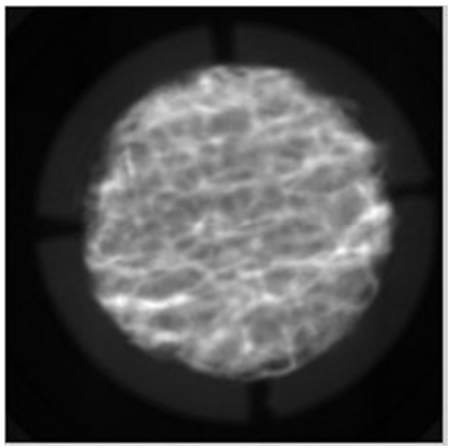

No 1 Elastic Modulus =126.0714
Strength =0.8987
BV/TV =0.1358

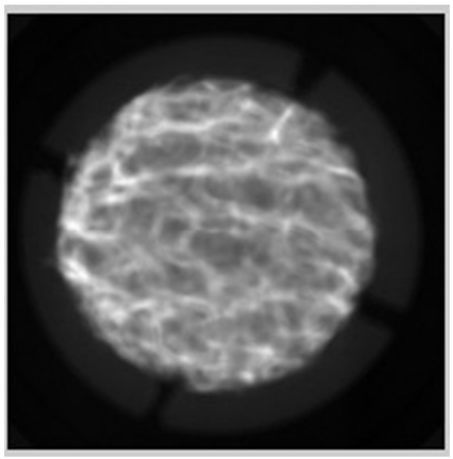

No 2 Elastic Modulus =226.4135
Strength =1.3178
BV/TV =0.1474

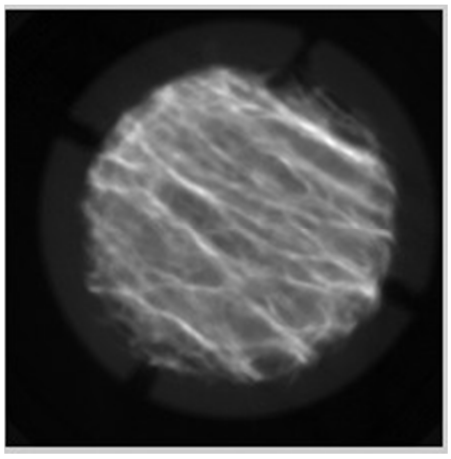

No 3 Elastic Modulus =119.7226
Strength =0.7369
BV/TV =0.1317

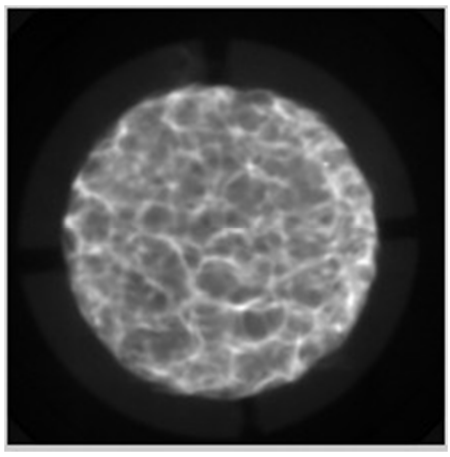

No 4 Elastic Modulus =693.0833
Strength =3.5748
BV/TV =0.1661

Appendix B (continued)

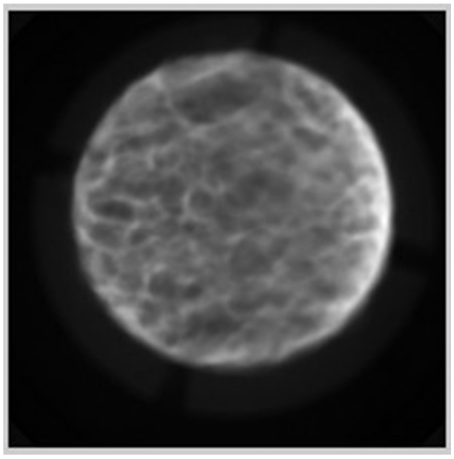

No 5 Elastic Modulus =552.2352
Strength =3.9367
BV/TV =0.2578

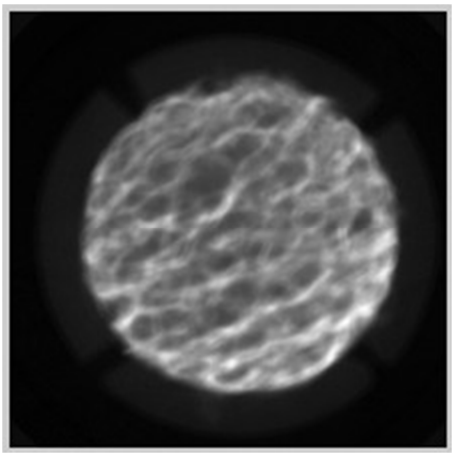

No 6 Elastic Modulus =516.5531
Strength =3.2789
BV/TV =0.1863

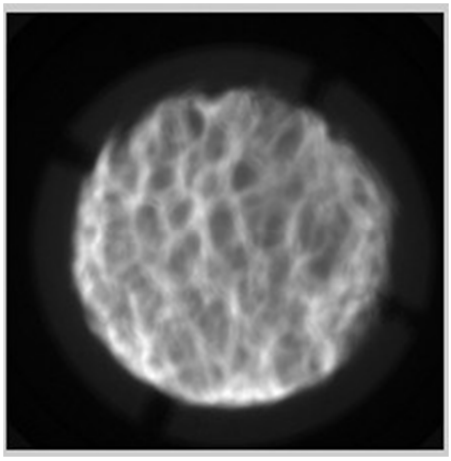

No 7 Elastic Modulus =427.3482
Strength =2.8928
BV/TV =0.1989

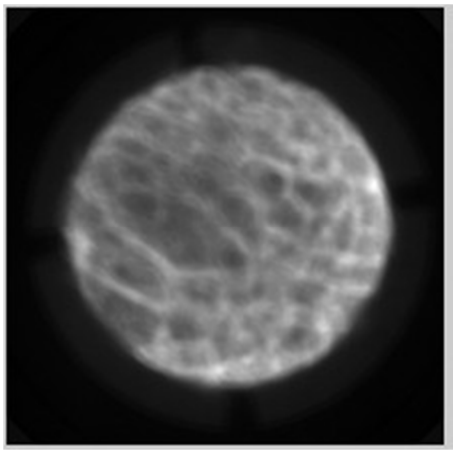

No 8 Elastic Modulus =534.8067
Strength =3.6252
BV/TV =0.2231

Appendix B (continued)

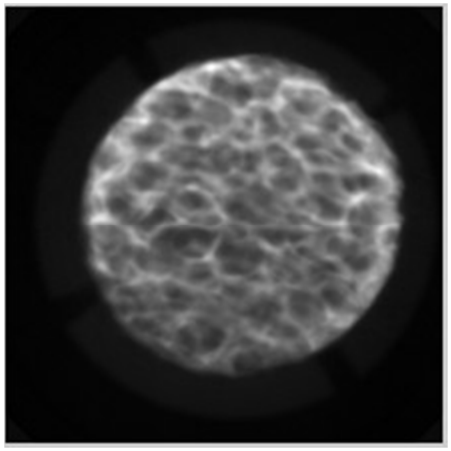

No 9 Elastic Modulus =1224.1592
Strength =7.5810
BV/TV =0.2153

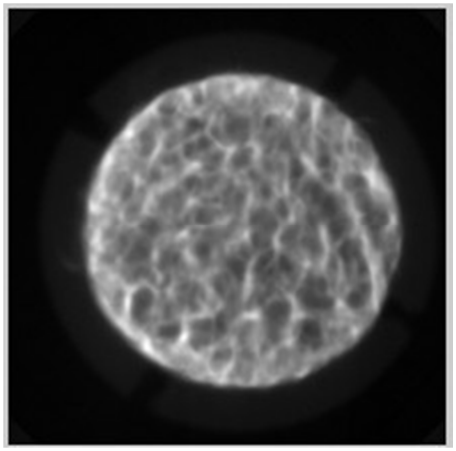

No 10 Elastic Modulus =1511.5543
Strength =7.0724
BV/TV =0.2327

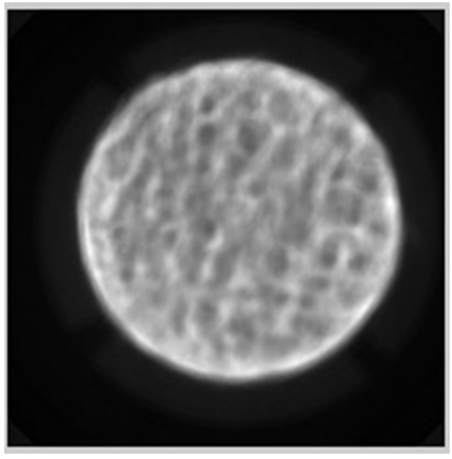

No 11 Elastic Modulus =1722.094
Strength =8.4276
BV/TV =0.3343

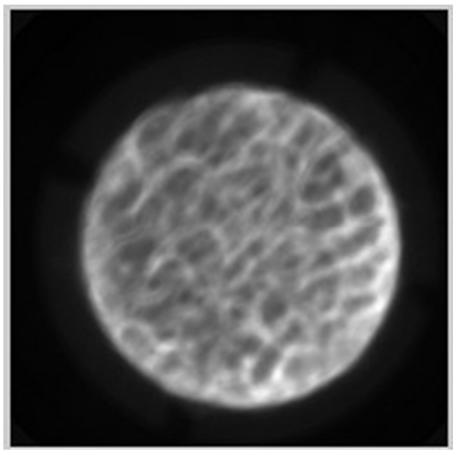

No 12 Elastic Modulus =1604.342
Strength =11.7123
BV/TV =0.3061

Appendix B (continued)

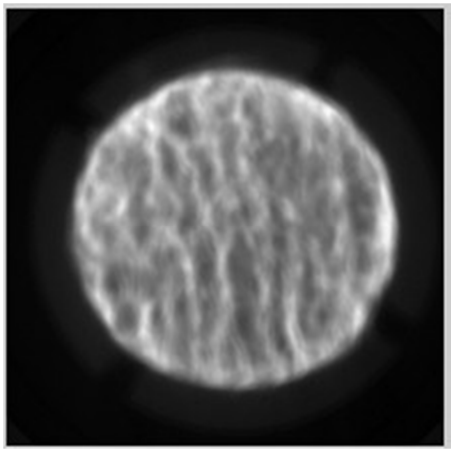

No 13 Elastic Modulus =1028.773
Strength =6.4984
BV/TV =0.2861

Appendix B (continued)

No	Elastic Modulus (MPa)	Strength (MPa)	BV/TV	Energy (d=1)				Energy(d=2)			
				A(θ=0)	A(θ=45)	A(θ=90)	A(θ=135)	A(θ=0)	A(θ=45)	A(θ=90)	A(θ=135)
1	126.0714	0.8987	0.1359	0.0662	0.0520	0.0564	0.0479	0.0453	0.0334	0.0371	0.0301
2	226.4135	1.3178	0.1475	0.0651	0.0475	0.0563	0.0508	0.0440	0.0295	0.0362	0.0318
3	119.7226	0.7370	0.1317	0.0647	0.0432	0.0556	0.0610	0.0440	0.0269	0.0361	0.0413
4	693.0833	3.5748	0.1661	0.0551	0.0420	0.0501	0.0426	0.0352	0.0255	0.0314	0.0260
5	552.2352	3.9367	0.2578	0.0674	0.0529	0.0593	0.0513	0.0463	0.0347	0.0394	0.0338
6	516.5530	3.2789	0.1863	0.0596	0.0526	0.0520	0.0401	0.0392	0.0340	0.0329	0.0245
7	427.3482	2.8929	0.1990	0.0595	0.0546	0.0728	0.0533	0.0391	0.0351	0.0511	0.0343
8	534.8067	3.6252	0.2230	0.0707	0.0540	0.0665	0.0619	0.0485	0.0356	0.0452	0.0412
9	1224.1590	7.5810	0.2153	0.0609	0.0445	0.0533	0.0484	0.0404	0.0281	0.0342	0.0309
10	1511.5545	7.0724	0.2328	0.0507	0.0439	0.0588	0.0431	0.0317	0.0270	0.0383	0.0266
11	1722.0936	8.4276	0.3344	0.0545	0.0499	0.0626	0.0453	0.0347	0.0307	0.0413	0.0273
12	1604.3418	11.7123	0.3061	0.0611	0.0557	0.0610	0.0465	0.0403	0.0360	0.0402	0.0292
13	1028.7697	6.4985	0.2861	0.0523	0.0460	0.0719	0.0500	0.0329	0.0281	0.0498	0.0309

No	Elastic Modulus (MPa)	Strength (MPa)	BV/TV	Energy(d=3)				Energy(d=4)			
				A(θ=0)	A(θ=45)	A(θ=90)	A(θ=135)	A(θ=0)	A(θ=45)	A(θ=90)	A(θ=135)
1	126.0714	0.8987	0.1359	0.0348	0.0255	0.0280	0.0228	0.0286	0.0217	0.0232	0.0196
2	226.4135	1.3178	0.1475	0.0337	0.0221	0.0267	0.0238	0.0277	0.0189	0.0217	0.0201
3	119.7226	0.7370	0.1317	0.0338	0.0210	0.0272	0.0325	0.0281	0.0187	0.0227	0.0276
4	693.0833	3.5748	0.1661	0.0264	0.0198	0.0234	0.0201	0.0219	0.0176	0.0196	0.0178
5	552.2352	3.9367	0.2578	0.0362	0.0270	0.0307	0.0268	0.0304	0.0232	0.0262	0.0234
6	516.5530	3.2789	0.1863	0.0298	0.0262	0.0245	0.0189	0.0246	0.0221	0.0203	0.0168
7	427.3482	2.8929	0.1990	0.0294	0.0266	0.0400	0.0262	0.0240	0.0222	0.0335	0.0220
8	534.8067	3.6252	0.2230	0.0378	0.0277	0.0351	0.0320	0.0316	0.0235	0.0293	0.0271
9	1224.1590	7.5810	0.2153	0.0310	0.0219	0.0259	0.0236	0.0257	0.0192	0.0217	0.0200
10	1511.5545	7.0724	0.2328	0.0237	0.0207	0.0293	0.0206	0.0198	0.0179	0.0244	0.0182
11	1722.0936	8.4276	0.3344	0.0255	0.0229	0.0307	0.0204	0.0209	0.0194	0.0250	0.0179
12	1604.3418	11.7123	0.3061	0.0304	0.0276	0.0306	0.0223	0.0251	0.0233	0.0251	0.0193
13	1028.7697	6.4985	0.2861	0.0242	0.0211	0.0383	0.0231	0.0199	0.0180	0.0315	0.0195

Appendix B (continued)

No	Elastic Modulus (MPa)	Strength (MPa)	BV/TV	Contrast(d=1)				Contrast(d=2)			
				C(θ=0)	C(θ=45)	C(θ=90)	C(θ=135)	C(θ=0)	C(θ=45)	C(θ=90)	C(θ=135)
1	126.0714	0.8987	0.1359	0.3898	0.7447	0.6029	0.9137	1.0475	2.1329	1.7529	2.6430
2	226.4135	1.3178	0.1475	0.4247	0.9120	0.5935	0.7958	1.1695	2.6444	1.7393	2.3000
3	119.7226	0.7370	0.1317	0.4206	1.2173	0.6326	0.5057	1.1409	3.3937	1.8324	1.3491
4	693.0833	3.5748	0.1661	0.6441	1.2123	0.7785	1.2152	1.8463	3.4514	2.2885	3.4388
5	552.2352	3.9367	0.2578	0.5327	0.9376	0.5949	0.9586	1.4465	2.5018	1.7451	2.6460
6	516.5530	3.2789	0.1863	0.5299	0.7484	0.7202	1.3585	1.4934	2.1199	2.1217	3.8392
7	427.3482	2.8929	0.1990	0.5208	0.7004	0.3458	0.7219	1.4777	1.9917	0.9019	2.0454
8	534.8067	3.6252	0.2230	0.3518	0.6794	0.3912	0.5087	0.9194	1.8929	1.0588	1.4167
9	1224.1590	7.5810	0.2153	0.4828	0.9844	0.6528	0.9092	1.3520	2.8411	1.8612	2.4225
10	1511.5545	7.0724	0.2328	0.7680	1.1291	0.5827	1.1819	2.3165	3.2893	1.6570	3.3585
11	1722.0936	8.4276	0.3344	0.6701	0.9042	0.5218	1.1260	2.0082	2.6620	1.4897	3.3547
12	1604.3418	11.7123	0.3061	0.5254	0.7059	0.4958	0.9886	1.5057	2.0471	1.4126	2.8694
13	1028.7697	6.4985	0.2861	0.6876	0.9614	0.3644	0.8305	2.0681	2.8962	0.9901	2.4719
No	Elastic Modulus (MPa)	Strength (MPa)	BV/TV	Contrast(d=3)				Contrast(d=4)			
				C(θ=0)	C(θ=45)	C(θ=90)	C(θ=135)	C(θ=0)	C(θ=45)	C(θ=90)	C(θ=135)
1	126.0714	0.8987	0.1359	1.9147	3.6864	3.1575	4.5109	2.8420	5.0487	4.5310	6.0993
2	226.4135	1.3178	0.1475	2.1353	4.5427	3.1861	3.9912	3.1329	6.1968	4.6562	5.5137
3	119.7226	0.7370	0.1317	2.0788	5.5042	3.2953	2.2887	3.0721	7.1122	4.7146	3.1733
4	693.0833	3.5748	0.1661	3.2689	5.6063	4.0493	5.5442	4.5946	7.2279	5.6638	7.1134
5	552.2352	3.9367	0.2578	2.3959	3.9446	3.1522	4.2162	3.2692	5.0723	4.4422	5.4460
6	516.5530	3.2789	0.1863	2.6824	3.5947	3.8223	6.2281	3.8626	4.8306	5.4492	8.0460
7	427.3482	2.8929	0.1990	2.7098	3.4617	1.6137	3.5213	4.0029	4.7755	2.3303	4.8076
8	534.8067	3.6252	0.2230	1.6526	3.2420	1.9483	2.4952	2.4192	4.3995	2.9002	3.4464
9	1224.1590	7.5810	0.2153	2.4353	4.7239	3.2899	3.9526	3.4969	6.1230	4.6408	5.2744
10	1511.5545	7.0724	0.2328	4.2021	5.4505	2.9099	5.4349	5.9574	7.1798	4.0575	6.9919
11	1722.0936	8.4276	0.3344	3.7468	4.6809	2.7554	5.8854	5.5490	6.3907	4.0995	7.9539
12	1604.3418	11.7123	0.3061	2.7745	3.5394	2.6296	4.7834	4.0587	4.7512	3.8815	6.2359
13	1028.7697	6.4985	0.2861	3.8617	5.1622	1.8396	4.4408	5.7261	7.1844	2.7862	6.2121

Appendix B (continued)

No	Elastic Modulus (MPa)	Strength (MPa)	BV/TV	Entropy(d=1)				Entropy(d=2)			
				E(θ=0)	E(θ=45)	E(θ=90)	E(θ=135)	E(θ=0)	E(θ=45)	E(θ=90)	E(θ=135)
1	126.0714	0.8987	0.1359	2.9374	3.1994	3.1067	3.2809	3.3465	3.6386	3.5460	3.7208
2	226.4135	1.3178	0.1475	2.9715	3.2951	3.1125	3.2326	3.3895	3.7420	3.5639	3.6802
3	119.7226	0.7370	0.1317	2.9688	3.3958	3.1298	3.0384	3.3802	3.8115	3.5680	3.4428
4	693.0833	3.5748	0.1661	3.1383	3.4169	3.2328	3.4123	3.5858	3.8529	3.6873	3.8457
5	552.2352	3.9367	0.2578	2.9741	3.2223	3.0851	3.2533	3.3694	3.6408	3.5218	3.6705
6	516.5530	3.2789	0.1863	3.0607	3.1995	3.1951	3.4630	3.4932	3.6332	3.6499	3.8895
7	427.3482	2.8929	0.1990	3.0541	3.1580	2.8593	3.1835	3.4889	3.5914	3.2329	3.6215
8	534.8067	3.6252	0.2230	2.8867	3.1659	2.9434	3.0345	3.2740	3.5881	3.3514	3.4439
9	1224.1590	7.5810	0.2153	3.0305	3.3390	3.1579	3.2765	3.4576	3.7769	3.6014	3.7008
10	1511.5545	7.0724	0.2328	3.2268	3.3821	3.0852	3.3961	3.6882	3.8242	3.5188	3.8303
11	1722.0936	8.4276	0.3344	3.1595	3.2637	3.0295	3.3664	3.6197	3.7168	3.4555	3.8237
12	1604.3418	11.7123	0.3061	3.0451	3.1552	3.0353	3.3174	3.4793	3.5920	3.4699	3.7599
13	1028.7697	6.4985	0.2861	3.1825	3.3209	2.8877	3.2465	3.6455	3.7810	3.2740	3.7052

No	Elastic Modulus (MPa)	Strength (MPa)	BV/TV	Entropy(d=3)				Entropy(d=4)			
				E(θ=0)	E(θ=45)	E(θ=90)	E(θ=135)	E(θ=0)	E(θ=45)	E(θ=90)	E(θ=135)
1	126.0714	0.8987	0.1359	3.6020	3.8549	3.7841	3.9266	3.7657	3.9667	3.9184	4.0226
2	226.4135	1.3178	0.1475	3.6430	3.9532	3.8161	3.9003	3.8012	4.0528	3.9601	4.0117
3	119.7226	0.7370	0.1317	3.6287	3.9806	3.8029	3.6633	3.7853	4.0493	3.9316	3.7955
4	693.0833	3.5748	0.1661	3.8253	4.0262	3.9158	4.0193	3.9587	4.0964	4.0324	4.0914
5	552.2352	3.9367	0.2578	3.5999	3.8422	3.7573	3.8599	3.7474	3.9462	3.8835	3.9518
6	516.5530	3.2789	0.1863	3.7401	3.8497	3.8868	4.0570	3.8892	3.9644	4.0141	4.1199
7	427.3482	2.8929	0.1990	3.7442	3.8155	3.4740	3.8451	3.8969	3.9378	3.6340	3.9639
8	534.8067	3.6252	0.2230	3.5184	3.8050	3.6000	3.6685	3.6806	3.9215	3.7570	3.7979
9	1224.1590	7.5810	0.2153	3.7025	3.9665	3.8372	3.9074	3.8509	4.0477	3.9662	4.0147
10	1511.5545	7.0724	0.2328	3.9190	4.0077	3.7560	4.0075	4.0329	4.0878	3.8953	4.0812
11	1722.0936	8.4276	0.3344	3.8725	3.9360	3.7174	4.0210	4.0079	4.0402	3.8768	4.0920
12	1604.3418	11.7123	0.3061	3.7351	3.8145	3.7265	3.9565	3.8858	3.9335	3.8803	4.0450
13	1028.7697	6.4985	0.2861	3.8957	3.9928	3.5274	3.9312	4.0294	4.0866	3.6970	4.0387

Appendix B (continued)

No	Elastic Modulus (MPa)	Strength (MPa)	BV/TV	Homogeneity(d=1)				Homogeneity(d=2)			
				H(θ=0)	H(θ=45)	H(θ=90)	H(θ=135)	H(θ=0)	H(θ=45)	H(θ=90)	H(θ=135)
1	126.0714	0.8987	0.1359	0.8306	0.7502	0.7745	0.7172	0.7043	0.5971	0.6251	0.5561
2	226.4135	1.3178	0.1475	0.8269	0.7205	0.7784	0.7468	0.7004	0.5614	0.6291	0.5911
3	119.7226	0.7370	0.1317	0.8257	0.6858	0.7732	0.8096	0.6996	0.5257	0.6261	0.6831
4	693.0833	3.5748	0.1661	0.7757	0.6844	0.7443	0.6891	0.6240	0.5193	0.5858	0.5248
5	552.2352	3.9367	0.2578	0.8348	0.7584	0.7944	0.7460	0.7151	0.6115	0.6525	0.5984
6	516.5530	3.2789	0.1863	0.8010	0.7616	0.7566	0.6685	0.6637	0.6162	0.6026	0.5015
7	427.3482	2.8929	0.1990	0.7981	0.7716	0.8600	0.7638	0.6582	0.6255	0.7520	0.6171
8	534.8067	3.6252	0.2230	0.8532	0.7715	0.8351	0.8145	0.7382	0.6320	0.7129	0.6864
9	1224.1590	7.5810	0.2153	0.8095	0.7057	0.7661	0.7353	0.6733	0.5449	0.6125	0.5823
10	1511.5545	7.0724	0.2328	0.7496	0.7025	0.7971	0.6936	0.5931	0.5406	0.6560	0.5294
11	1722.0936	8.4276	0.3344	0.7696	0.7430	0.8155	0.7073	0.6167	0.5800	0.6807	0.5378
12	1604.3418	11.7123	0.3061	0.8064	0.7780	0.8074	0.7163	0.6663	0.6309	0.6674	0.5546
13	1028.7697	6.4985	0.2861	0.7576	0.7135	0.8568	0.7454	0.5972	0.5453	0.7466	0.5823
No	Elastic Modulus (MPa)	Strength (MPa)	BV/TV	Homogeneity(d=3)				Homogeneity(d=4)			
				H(θ=0)	H(θ=45)	H(θ=90)	H(θ=135)	H(θ=0)	H(θ=45)	H(θ=90)	H(θ=135)
1	126.0714	0.8987	0.1359	0.6141	0.5067	0.5295	0.4600	0.5494	0.4506	0.4637	0.4051
2	226.4135	1.3178	0.1475	0.6123	0.4667	0.5298	0.4951	0.5489	0.4107	0.4624	0.4333
3	119.7226	0.7370	0.1317	0.6107	0.4399	0.5311	0.6018	0.5473	0.3928	0.4681	0.5465
4	693.0833	3.5748	0.1661	0.5279	0.4346	0.4894	0.4413	0.4685	0.3847	0.4336	0.3941
5	552.2352	3.9367	0.2578	0.6317	0.5233	0.5617	0.5153	0.5715	0.4714	0.5054	0.4632
6	516.5530	3.2789	0.1863	0.5728	0.5295	0.5067	0.4106	0.5094	0.4726	0.4425	0.3574
7	427.3482	2.8929	0.1990	0.5655	0.5335	0.6712	0.5271	0.5002	0.4699	0.6109	0.4682
8	534.8067	3.6252	0.2230	0.6541	0.5454	0.6284	0.6022	0.5928	0.4899	0.5683	0.5455
9	1224.1590	7.5810	0.2153	0.5811	0.4617	0.5179	0.4922	0.5194	0.4160	0.4575	0.4343
10	1511.5545	7.0724	0.2328	0.4976	0.4507	0.5665	0.4414	0.4378	0.3952	0.5055	0.3949
11	1722.0936	8.4276	0.3344	0.5160	0.4811	0.5820	0.4365	0.4458	0.4205	0.5128	0.3782
12	1604.3418	11.7123	0.3061	0.5690	0.5401	0.5737	0.4629	0.5026	0.4841	0.5069	0.4109
13	1028.7697	6.4985	0.2861	0.4949	0.4477	0.6614	0.4822	0.4256	0.3858	0.5969	0.4193

Appendix B (continued)

No	Elastic Modulus (MPa)	Strength (MPa)	BV/TV	Autocorrelation(d=1)				Autocorrelation(d=2)			
				U(θ=0)	U(θ=45)	U(θ=90)	U(θ=135)	U(θ=0)	U(θ=45)	U(θ=90)	U(θ=135)
1	126.0714	0.8987	0.1359	25.9160	25.8206	25.8158	25.7606	25.7946	25.4175	25.4531	25.2093
2	226.4135	1.3178	0.1475	25.8706	25.7135	25.7938	25.7781	25.7067	25.1435	25.4385	25.3201
3	119.7226	0.7370	0.1317	25.6577	25.3399	25.5556	25.7226	25.5173	24.5444	25.1683	25.6161
4	693.0833	3.5748	0.1661	25.6957	25.5010	25.6310	25.5008	25.2962	24.6534	25.0741	24.6585
5	552.2352	3.9367	0.2578	25.8398	25.7239	25.8099	25.7113	25.5563	25.1179	25.4316	25.0721
6	516.5530	3.2789	0.1863	25.7138	25.6781	25.6099	25.3851	25.4383	25.2604	25.1057	24.3890
7	427.3482	2.8929	0.1990	25.6246	25.6145	25.7025	25.6001	25.3532	25.2515	25.6241	25.2139
8	534.8067	3.6252	0.2230	25.7549	25.6691	25.7376	25.7557	25.6683	25.3225	25.6052	25.5769
9	1224.1590	7.5810	0.2153	25.7675	25.5993	25.6843	25.6321	25.5245	24.9240	25.2615	25.0220
10	1511.5545	7.0724	0.2328	25.5892	25.4944	25.6831	25.4639	25.0113	24.6604	25.3411	24.5956
11	1722.0936	8.4276	0.3344	25.6163	25.5817	25.6905	25.4684	25.1434	24.9815	25.4029	24.6283
12	1604.3418	11.7123	0.3061	25.6636	25.6572	25.6760	25.5134	25.3708	25.2620	25.4132	24.8341
13	1028.7697	6.4985	0.2861	25.5547	25.4983	25.7128	25.5603	25.0598	24.8076	25.5956	25.0133

No	Elastic Modulus (MPa)	Strength (MPa)	BV/TV	Autocorrelation(d=3)				Autocorrelation(d=4)			
				U(θ=0)	U(θ=45)	U(θ=90)	U(θ=135)	U(θ=0)	U(θ=45)	U(θ=90)	U(θ=135)
1	126.0714	0.8987	0.1359	25.5712	24.9098	24.9592	24.5823	25.3111	24.4442	24.4674	24.0726
2	226.4135	1.3178	0.1475	25.4280	24.4664	24.9290	24.7101	25.1074	23.8622	24.3901	24.1080
3	119.7226	0.7370	0.1317	25.2545	23.7631	24.6403	25.4069	24.9366	23.2007	24.1131	25.1610
4	693.0833	3.5748	0.1661	24.7483	23.7550	24.3759	23.7638	24.1856	23.0041	23.7151	23.0126
5	552.2352	3.9367	0.2578	25.1241	24.3528	24.8746	24.2785	24.6300	23.6258	24.2641	23.5305
6	516.5530	3.2789	0.1863	25.0067	24.6744	24.4098	23.2687	24.4993	24.0632	23.6765	22.3121
7	427.3482	2.8929	0.1990	24.9359	24.7290	25.4534	24.6888	24.4559	24.1730	25.2285	24.1656
8	534.8067	3.6252	0.2230	25.4769	24.8211	25.3536	25.2562	25.2205	24.2945	25.0363	24.8665
9	1224.1590	7.5810	0.2153	25.1099	24.1236	24.6695	24.2627	24.6167	23.4394	24.0663	23.5338
10	1511.5545	7.0724	0.2328	24.2288	23.6407	24.8319	23.5933	23.4197	22.6672	24.2606	22.7184
11	1722.0936	8.4276	0.3344	24.4564	24.1566	24.9627	23.5690	23.6780	23.2669	24.4454	22.5220
12	1604.3418	11.7123	0.3061	24.9079	24.6832	24.9848	24.0001	24.3632	24.0458	24.4732	23.2524
13	1028.7697	6.4985	0.2861	24.3473	23.8726	25.3652	24.2477	23.5482	22.8910	25.0619	23.4062

Appendix B (continued)

No	Elastic Modulus (MPa)	Strength (MPa)	BV/TV	Correlation(d=1)				Correlation(d=2)			
				R(θ=0)	R(θ=45)	R(θ=90)	R(θ=135)	R(θ=0)	R(θ=45)	R(θ=90)	R(θ=135)
1	126.0714	0.8987	0.1359	0.1845	0.1788	0.1806	0.1759	0.1743	0.1550	0.1611	0.1455
2	226.4135	1.3178	0.1475	0.1839	0.1758	0.1809	0.1780	0.1721	0.1452	0.1614	0.1518
3	119.7226	0.7370	0.1317	0.1849	0.1708	0.1810	0.1844	0.1734	0.1311	0.1602	0.1709
4	693.0833	3.5748	0.1661	0.1817	0.1718	0.1792	0.1717	0.1605	0.1302	0.1520	0.1304
5	552.2352	3.9367	0.2578	0.1843	0.1774	0.1831	0.1770	0.1680	0.1483	0.1628	0.1455
6	516.5530	3.2789	0.1863	0.1827	0.1793	0.1791	0.1680	0.1663	0.1551	0.1543	0.1221
7	427.3482	2.8929	0.1990	0.1837	0.1811	0.1869	0.1807	0.1675	0.1585	0.1783	0.1575
8	534.8067	3.6252	0.2230	0.1860	0.1807	0.1853	0.1839	0.1772	0.1595	0.1747	0.1690
9	1224.1590	7.5810	0.2153	0.1849	0.1762	0.1816	0.1773	0.1697	0.1418	0.1600	0.1492
10	1511.5545	7.0724	0.2328	0.1783	0.1724	0.1818	0.1713	0.1507	0.1326	0.1631	0.1312
11	1722.0936	8.4276	0.3344	0.1800	0.1764	0.1827	0.1722	0.1565	0.1450	0.1664	0.1317
12	1604.3418	11.7123	0.3061	0.1833	0.1807	0.1838	0.1754	0.1666	0.1572	0.1683	0.1411
13	1028.7697	6.4985	0.2861	0.1802	0.1758	0.1862	0.1783	0.1558	0.1407	0.1763	0.1490

No	Elastic Modulus (MPa)	Strength (MPa)	BV/TV	Correlation(d=3)				Correlation(d=4)			
				R(θ=0)	R(θ=45)	R(θ=90)	R(θ=135)	R(θ=0)	R(θ=45)	R(θ=90)	R(θ=135)
1	126.0714	0.8987	0.1359	0.1595	0.1259	0.1355	0.1098	0.1426	0.0990	0.1092	0.0774
2	226.4135	1.3178	0.1475	0.1551	0.1090	0.1351	0.1198	0.1365	0.0759	0.1068	0.0898
3	119.7226	0.7370	0.1317	0.1567	0.0900	0.1331	0.1539	0.1380	0.0570	0.1056	0.1369
4	693.0833	3.5748	0.1661	0.1338	0.0880	0.1186	0.0892	0.1080	0.0554	0.0868	0.0576
5	552.2352	3.9367	0.2578	0.1501	0.1206	0.1359	0.1152	0.1336	0.0986	0.1108	0.0913
6	516.5530	3.2789	0.1863	0.1443	0.1270	0.1225	0.0764	0.1218	0.1032	0.0913	0.0410
7	427.3482	2.8929	0.1990	0.1449	0.1306	0.1659	0.1294	0.1198	0.1047	0.1527	0.1039
8	534.8067	3.6252	0.2230	0.1644	0.1340	0.1589	0.1488	0.1502	0.1117	0.1408	0.1303
9	1224.1590	7.5810	0.2153	0.1491	0.1054	0.1331	0.1202	0.1287	0.0782	0.1070	0.0947
10	1511.5545	7.0724	0.2328	0.1152	0.0913	0.1396	0.0916	0.0817	0.0581	0.1179	0.0617
11	1722.0936	8.4276	0.3344	0.1241	0.1062	0.1434	0.0827	0.0893	0.0727	0.1176	0.0419
12	1604.3418	11.7123	0.3061	0.1431	0.1284	0.1459	0.1042	0.1184	0.1048	0.1218	0.0758
13	1028.7697	6.4985	0.2861	0.1221	0.0968	0.1615	0.1110	0.0858	0.0568	0.1436	0.0760

Appendix B (continued)

No	Elastic Modulus (MPa)	Strength (MPa)	BV/TV	Cluster Shade(d=1)				Cluster Shade(d=2)			
				S(θ=0)	S(θ=45)	S(θ=90)	S(θ=135)	S(θ=0)	S(θ=45)	S(θ=90)	S(θ=135)
1	126.0714	0.8987	0.1359	-3.5277	-4.3428	-4.1993	-4.8301	-4.5436	-6.4913	-6.5841	-7.4183
2	226.4135	1.3178	0.1475	-2.6035	-3.3714	-3.2265	-3.4193	-3.1150	-4.5040	-4.8933	-5.2151
3	119.7226	0.7370	0.1317	-1.7070	-4.3675	-2.6297	-1.8464	-3.3487	-9.2675	-5.9878	-3.3445
4	693.0833	3.5748	0.1661	-3.9669	-4.6441	-4.4811	-4.6617	-4.5132	-5.7201	-5.8198	-5.6243
5	552.2352	3.9367	0.2578	-3.0414	-2.4275	-2.5973	-2.2821	-2.5938	-0.7319	-0.6155	-0.3255
6	516.5530	3.2789	0.1863	-2.0127	-1.9187	-2.2944	-2.5376	-1.9537	-1.6194	-2.6181	-3.2647
7	427.3482	2.8929	0.1990	-2.0281	-2.3073	-1.6940	-1.9813	-2.9209	-3.5374	-1.9925	-2.4501
8	534.8067	3.6252	0.2230	-2.4227	-2.6109	-2.4824	-2.6560	-2.7760	-3.1835	-2.8534	-3.0917
9	1224.1590	7.5810	0.2153	-2.3615	-2.4218	-2.3377	-2.2615	-2.3972	-2.2576	-2.1787	-2.2850
10	1511.5545	7.0724	0.2328	-0.9873	-0.8378	-0.5734	-0.9648	-1.4912	-1.0320	-0.5350	-1.5219
11	1722.0936	8.4276	0.3344	-1.5036	-1.5305	-1.6504	-1.2614	-0.6968	-0.6168	-1.2851	0.6431
12	1604.3418	11.7123	0.3061	-1.1720	-1.0699	-1.1477	-0.8431	-0.4679	-0.1383	-0.4212	0.6611
13	1028.7697	6.4985	0.2861	-1.9516	-2.0713	-1.9252	-1.8469	-1.9125	-1.8392	-1.8604	-1.1444
No	Elastic Modulus (MPa)	Strength (MPa)	BV/TV	Cluster Shade(d=3)				Cluster Shade(d=4)			
				S(θ=0)	S(θ=45)	S(θ=90)	S(θ=135)	S(θ=0)	S(θ=45)	S(θ=90)	S(θ=135)
1	126.0714	0.8987	0.1359	-5.2178	-8.0946	-8.7704	-8.9028	-5.4480	-8.7097	-10.2707	-9.3453
2	226.4135	1.3178	0.1475	-3.4435	-4.5705	-6.1319	-6.7522	-3.6463	-3.9412	-6.7593	-7.7674
3	119.7226	0.7370	0.1317	-5.1401	-11.7378	-9.0882	-4.8802	-6.7673	-11.8391	-11.2396	-6.1499
4	693.0833	3.5748	0.1661	-4.8500	-6.0559	-6.5061	-5.3407	-4.7208	-5.5008	-6.2921	-4.1544
5	552.2352	3.9367	0.2578	-2.0262	1.5602	1.4790	2.3293	-1.2693	3.7696	3.6056	5.1706
6	516.5530	3.2789	0.1863	-1.9630	-1.3790	-2.7295	-3.4717	-1.9346	-0.5858	-2.5184	-2.8541
7	427.3482	2.8929	0.1990	-3.6486	-4.7619	-2.3476	-2.6711	-4.2493	-5.4187	-2.5872	-2.5654
8	534.8067	3.6252	0.2230	-3.1821	-3.3988	-3.1744	-4.0383	-3.4565	-2.6965	-3.4833	-4.9019
9	1224.1590	7.5810	0.2153	-2.7738	-1.6794	-1.7079	-2.1142	-3.0646	-0.8494	-1.1381	-2.1623
10	1511.5545	7.0724	0.2328	-1.7275	-0.8413	-0.7638	-1.2039	-1.4639	0.1288	-0.5999	-0.2276
11	1722.0936	8.4276	0.3344	0.6343	-0.0516	-0.4449	2.7829	2.1069	0.6244	0.2742	4.8383
12	1604.3418	11.7123	0.3061	0.5546	0.3282	0.5060	2.4364	1.5522	1.2671	1.3951	3.8928
13	1028.7697	6.4985	0.2861	-1.2493	-1.3635	-1.5775	-0.0293	-0.2298	-0.2882	-1.4649	1.7581

Appendix C

GLCM Distribution for Different Level Strength Bones

Weak bone

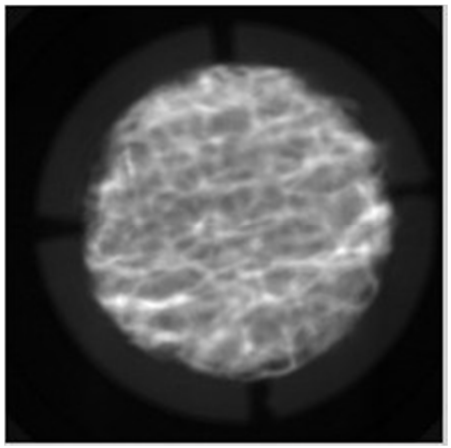

Elastic modulus	Strength	BV/TV
126.071	0.899	0.136

Degree=0, Displacement=1

2107	197	4	1	0	0	0	0
198	1676	405	33	6	0	0	0
4	415	1644	480	47	2	0	0
0	28	493	1203	515	62	3	0
0	2	43	535	1324	543	32	0
0	0	2	47	559	1506	509	12
0	0	1	5	27	515	1520	346
0	0	0	0	1	7	350	2237

Degree=45, Displacement=1

1968	246	22	6	3	0	0	0
241	1440	550	72	12	2	1	0
26	513	1284	576	154	31	8	0
9	80	543	898	603	152	19	0
1	33	158	536	943	690	110	8
0	6	26	184	603	1099	660	57
0	0	9	31	151	569	1110	544
0	0	0	1	10	92	506	1986

Appendix C (Continued)

Degree=90, Displacement=1

2103	183	16	2	0	0	0	0
196	1581	460	64	15	2	0	0
5	505	1393	543	131	11	4	0
0	47	563	962	579	143	10	0
0	2	143	590	988	631	121	4
0	0	13	139	673	1179	570	61
0	0	4	4	93	630	1195	488
0	0	0	0	0	39	514	2042

Degree=135, Displacement=1

1946	235	37	5	3	0	0	0
265	1365	509	135	36	5	3	0
14	594	1135	570	225	48	6	0
1	104	612	737	570	236	43	1
0	17	247	577	796	636	180	26
0	2	45	247	630	976	623	112
0	1	6	33	207	622	992	553
0	0	1	0	12	112	567	1903

Appendix C (Continued)

Median bone

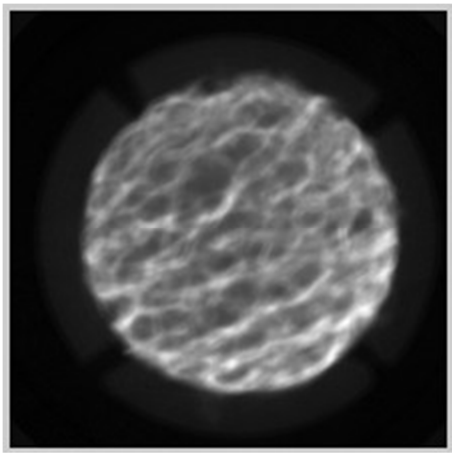

Elastic modulus	Strength	BV/TV
516.553	3.279	0.186

Degree=0, Displacement=1

1959	331	38	5	1	0	0	0
315	1555	490	56	12	0	0	0
40	467	1433	576	81	20	0	0
13	50	559	1146	572	74	9	0
6	15	79	546	1312	591	47	0
1	8	12	79	561	1286	508	8
0	2	6	13	52	469	1713	391
0	0	0	2	5	23	369	2158

Degree=45, Displacement=1

1799	365	68	35	5	4	0	0
381	1427	503	60	33	20	3	0
65	516	1259	592	135	39	11	0
18	85	588	1033	553	121	20	5
11	25	162	550	1157	587	101	3
1	9	29	131	611	1107	545	30
0	1	8	22	98	554	1516	447
0	0	0	0	4	31	450	2072

Appendix C (Continued)

Degree=90, Displacement=1

1919	366	50	5	1	0	0	0
350	1426	547	82	23	0	0	0
46	534	1226	590	186	28	7	0
20	73	585	1007	570	156	12	0
5	14	170	566	1104	610	124	3
0	12	31	149	604	1050	586	31
1	3	7	23	103	576	1435	498
0	0	1	1	5	43	482	2025

Degree=135, Displacement=1

1657	434	129	33	15	0	0	0
438	1111	566	205	83	19	4	0
93	621	917	541	298	113	32	1
36	169	589	742	539	272	73	3
20	53	285	554	823	584	248	29
14	17	100	257	589	755	597	134
6	19	24	74	214	586	1107	616
3	2	7	17	35	134	585	1774

Appendix C (Continued)

Strong bone

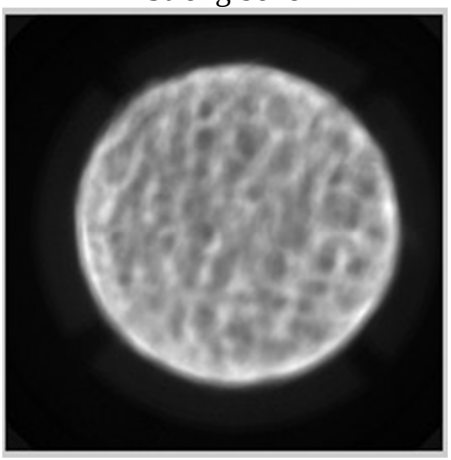

Elastic modulus	Strength	BV/TV
1722.093	8.428	0.334

Degree=0, Displacement=1

2029	399	42	23	11	0	0	0
397	1524	533	107	23	17	2	0
52	560	1153	633	101	26	1	0
21	92	651	1310	673	114	21	0
2	23	121	658	1084	651	70	4
3	5	25	138	620	1328	581	48
0	0	1	13	93	563	1509	412
0	0	0	0	8	49	407	2329

Degree=45, Displacement=1

1848	444	62	42	26	11	1	0
433	1440	556	100	20	42	12	0
82	548	1086	639	116	29	22	4
42	116	647	1254	674	107	22	20
19	33	131	669	991	665	81	24
10	20	32	144	649	1228	571	94
0	2	12	30	122	602	1385	438
0	0	0	4	15	64	497	2213

Appendix C (Continued)

Degree=90, Displacement=1

2097	338	38	25	6	0	0	0
337	1736	455	47	19	9	0	0
51	431	1419	568	38	19	0	0
18	54	536	1609	595	56	14	0
1	25	38	562	1372	575	39	1
0	19	29	47	548	1573	510	22
0	0	11	22	19	457	1710	372
0	0	0	2	16	59	318	2398

Degree=135, Displacement=1

1792	451	104	53	24	12	0	0
471	1300	538	211	38	34	10	1
94	591	940	639	205	47	10	0
40	169	652	1066	674	234	41	6
25	41	207	629	871	670	163	7
13	36	64	224	607	1071	637	96
1	14	8	39	172	565	1285	507
0	1	13	21	22	115	445	2176